A stable and adaptive semi-Lagrangian potential model for unsteady and nonlinear ship-wave interactions

Andrea Mola[a], Luca Heltai[a,1], Antonio DeSimone[a]

[a]*SISSA, International School for Advanced Studies, Via Bonomea 265, 34136 Trieste - Italy*

Abstract

We present an innovative numerical discretization of the equations of inviscid potential flow for the simulation of three dimensional unsteady and nonlinear water waves generated by a ship hull advancing in water.

The equations of motion are written in a semi-Lagrangian framework, and the resulting integro-differential equations are discretized in space via an adaptive iso-parametric collocation Boundary Element Method, and in time via adaptive implicit Backward Differentiation Formulas (BDF) with variable step and variable order.

When the velocity of the advancing ship hull is non-negligible, the semi-Lagrangian formulation (also known as Arbitrary Lagrangian Eulerian formulation, or ALE) of the free surface equations contains dominant transport terms which are stabilized with a Streamwise Upwind Petrov-Galerkin (SUPG) method.

The SUPG stabilization allows automatic and robust adaptation of the spatial discretization with unstructured quadrilateral grids. Preliminary results are presented where we compare our numerical model with experimental results on the case of a Wigley hull advancing in calm water with fixed sink and trim.

Keywords: unsteady ship-wave interaction; nonlinear free surface problems; semi-Lagrangian formulation; arbitrary Lagrangian Eulerian formulation; boundary element method

*Corresponding author, Tel.: +39 040-3787449; Fax: +39 040-3787528

Email addresses: andrea.mola@sissa.it (Andrea Mola), luca.heltai@sissa.it (Luca Heltai), desimone@sissa.it (Antonio DeSimone)

1. Introduction

Over the last decades, the need for accurate prediction of the hydrodynamic performances of ships has led to the development of increasingly efficient and accurate models for the simulation of the three dimensional, nonlinear and unsteady water waves generated by a moving hull. In particular, models based on potential flow theory have historically been among the most successful in the simulation of the dynamics of nonbreaking waves. In this framework, the assumptions of irrotational flow and inviscid fluid reduce the Navier Stokes incompressibility constraint and momentum balance equations to the Laplace's and Bernoulli's equations, defined on a moving domain.

This boundary value problem is tackled with a Mixed Eulerian–Lagrangian approach, in which the Eulerian field equations are solved to obtain the fluid velocities, which are then used to displace in a Lagrangian way the free surface, and update the corresponding potential field values [23]. In this framework, the Eulerian problem is expressed in boundary integral form, and it is typically discretized using the Boundary Element Method (BEM). The velocity field and Bernoulli's equation provide a kinematic boundary condition for the Lagrangian evolution of the free surface, and a dynamic boundary condition for the evolution of the potential field.

Numerical treatments of the Lagrangian step usually rely on accurate reconstructions of position vector and potential field gradients, which may lead to instability in the time advancing scheme for the free surface discretization, as well as for the corresponding potential field values. A smoothing technique is typically adopted to reduce the sensitivity of the discretization on the reconstruction of the full velocity field, at the cost of introducing an artificial viscosity in the system.

An alternative cure was presented by Grilli et al. [12] who developed a high order iso-parametric BEM discretization of a Numerical Wave Tank to simulate overturning waves up to the breaking point on arbitrarily shaped bottoms. The use of a high order discretization bypasses the problem of reconstructing the gradients, and is very reliable when the numerical evolution of the free surface is done in a purely Lagrangian way.

Ship hydrodynamics simulations, however, are typically carried out in a frame of reference attached to the boat, requiring the presence of a water current in the simulations, which, in a fully Lagrangian approach, leads to downstream transportation of the free surface nodes, or to their clustering around stagnation points, ultimately resulting in blowup of the simulations (see, for example, [21]).

Beck [4] proposed alternative *semi-Lagrangian* free surface boundary conditions, under the assumption that the surface elevation function is single-valued. Employing such conditions, it is possible to prescribe the horizontal velocity of the free surface nodes of the computational grid, and compute the vertical velocity needed to keep the nodes on the free surface. However, in presence of significant difference between the water current speed and the horizontal nodes speed, the semi-Lagrangian scheme has some dominant transport terms, and stability issues may arise [21], [20]. The semi-Lagrangian free surface boundary

conditions proposed by Beck have been in most cases employed imposing nodes longitudinal speeds equal to the water current ones, and lateral velocities chosen so that the nodes would follow prescribed horizontal paths [21].

More recently, Sung and Grilli [22] applied an alternative method, combining semi-Lagrangian and Lagrangian free surface boundary conditions to the problem of a pressure perturbation moving on the water surface, which was then tested on a Wigley hull. The semi-Lagrangian free surface boundary conditions were used also in the work of Kjellberg, Contento and Jansson [17], where free surface instabilities are avoided by choosing an earth fixed reference frame, in which no current speed is needed. The drawback of this choice is that in such frame the ship moves with a specified horizontal speed, and the computational grid needs to be constantly regenerated to cover the region surrounding the hull with an adequate number of cells.

The purpose of this work is to present new results obtained with a semi-Lagrangian potential model for the simulation of three dimensional unsteady nonlinear water waves generated by a ship hull advancing in calm water. The resulting integro-differential boundary value problem is discretized to a system of nonlinear differential-algebraic equations, in which the unknowns are the positions of the nodes of the computational grid, along with the corresponding potential and potential normal derivative values. Among these, the vertical positions and the potential values associated with the free surface nodes are differential components, while the other unknowns are purely algebraic.

Time advancing of the nonlinear differential-algebraic system is performed using implicit Backward Differentiation Formulas (BDF) with variable step size and variable order. At each time step, such method results in a nonlinear algebraic system, solved with Newton's method. Both the BDF and Newton's method are implemented in the framework of the open source library SUNDIALS [14] for the resolution of nonlinear differential-algebraic equations. The collocated and iso-parametric BEM discretization of the Laplace's equation has been implemented employing the open source C++ library deal.II [3].

The computational grid, composed by quadrilateral cells of arbitrary order, is adapted in a geometrically consistent way (see [6]) via an a posteriori error estimator based on the jump of the solution gradient along the cell internal boundaries. Even when low order boundary elements are used, accurate estimations of the position vector and potential gradients on the free surface are recovered by means of a Streamwise Upwind Petrov–Galerkin (SUPG) projection, which is used to stabilize the transport dominated terms. The SUPG projection is strongly consistent, and does not introduce numerical dissipation in the equations, allowing the use of robust unstructured grids, which can be generated and managed on arbitrary hull geometries in a relatively simple way.

The test case considered in this paper is that of a Wigley hull advancing at constant speed in calm water. The simulations have been performed using bilinear elements. The arbitrary horizontal velocity specified in the semi-Lagrangian free surface boundary condition is chosen so as to impose null longitudinal nodes velocity with respect to the hull. The simulations results obtained imposing six different Froude numbers are finally compared with experimental results re-

ported in [19], to assess the accuracy of the model.

2. Three dimensional potential model

The equations of motion that better describe the velocity and pressure fields $\boldsymbol{v}$ and p of a fluid region around a ship hull are the incompressible Navier–Stokes equations, written in the moving domain $\Omega(t) \subset \mathbb{R}^3$, which is a (simply connected) region of water surrounding the ship hull itself:

$$\rho\left(\frac{\partial \boldsymbol{v}}{\partial t} + \boldsymbol{v}\cdot\boldsymbol{\nabla}\boldsymbol{v}\right) = \boldsymbol{\nabla}\cdot\boldsymbol{\sigma} + \boldsymbol{b} \qquad \text{in } \Omega(t) \tag{1a}$$

$$\boldsymbol{\nabla}\cdot\boldsymbol{v} = 0 \qquad \text{in } \Omega(t) \tag{1b}$$

$$\boldsymbol{\sigma}\cdot\boldsymbol{n} = p_a\boldsymbol{n} \qquad \text{on } \Gamma^w(t) \tag{1c}$$

$$\boldsymbol{v} = \boldsymbol{v}_g \qquad \text{on } \Gamma(t)\setminus\Gamma^w(t) \tag{1d}$$

where ρ is the (constant) fluid density, $\boldsymbol{b}$ are external body forces (typically gravity and possibly other inertial forces due to a non inertial movement of the reference frame), $\boldsymbol{\sigma} = -p\boldsymbol{I} + \mu(\boldsymbol{\nabla}\boldsymbol{v} + \boldsymbol{\nabla}\boldsymbol{v}^T)$ is the stress tensor for an incompressible Newtonian fluid, $\Gamma(t) := \partial\Omega(t)$ is the boundary of the region of interest, and $\boldsymbol{n}$ is the outer normal to the boundary $\Gamma(t)$. On the free surface $\Gamma^w(t)$, the air is assumed to exert a constant atmospheric pressure p_a on the underlying water, and we neglect shear stresses due to the wind. On the other boundaries of the domain, the prescribed velocity $\boldsymbol{v}_g$ is either equal to the ship hull velocity, or to a given velocity field (for inflow and outflow boundary conditions far away from the ship hull itself).

Equation (1a) is usually referred to as the momentum balance equation, while (1b) is referred to as the incompressibility constraint, or continuity equation.

In the flow field past a slender ship hull, vorticity is confined to the boundary layer region and to a thin wake following the boat: in these conditions, the assumption of irrotational and non viscous flow is fairly accurate, and viscous effects can be recovered, if necessary, by other means such as empirical algebraic formulas, or —better— by the interface with a suitable boundary layer model.

For an irrotational and invishid flow, the velocity field $\boldsymbol{v}$ admits a representation through a scalar potential function $\Phi(\boldsymbol{x}, t)$, namely

$$\boldsymbol{v} = \boldsymbol{\nabla}\Phi \qquad \text{in } \ \Omega(t). \tag{2}$$

In this case, the equations of motion simplify to the unsteady Bernoulli equation and to the Laplace equation for the flow potential:

$$\frac{\partial\Phi}{\partial t} + \frac{1}{2}\left|\boldsymbol{\nabla}\Phi\right|^2 + \frac{p - p_a}{\rho} + \boldsymbol{\beta}\cdot\boldsymbol{x} = C(t) \qquad \text{in } \Omega(t) \tag{3a}$$

$$\Delta\Phi = 0 \qquad \text{in } \Omega(t) \tag{3b}$$

where $C(t)$ is an arbitrary function of time, and we have assumed that all body forces could be expressed as $\boldsymbol{b} = -\boldsymbol{\nabla}(\boldsymbol{\beta} \cdot \boldsymbol{x})$, i.e., they are all of potential type. This is true for gravitational body forces and for inertial body forces due to uniform accelerations along fixed directions of the frame of reference.

In this framework, the unknowns of the problem Φ and p are uncoupled, and it's possible to recover the pressure by postprocessing the solution of the Poisson problem (3b) via Bernoulli's Equation (3a).

Since arbitrary uniform variations of the potential field produce the same velocity field (i.e., $\boldsymbol{\nabla}(\Phi(\boldsymbol{x}, t) + C(t)) = \boldsymbol{\nabla}\Phi(\boldsymbol{x}, t)$), we can set $C(t) = 0$, and we can combine Bernoulli equation (3a) and the dynamic boundary condition on the free surface (1c) to obtain an evolution equation for the potential field $\Phi(\boldsymbol{x}, t)$ on the free surface $\Gamma^w(t)$.

The shape of the water domain $\Omega(t)$ is time dependent and it is part of the unknowns of the problems. The free surface $\Gamma^w(t)$ should move following the fluid velocity $\boldsymbol{v}$. In ship hydrodynamics, however, it is desirable to maintain the frame of reference attached to the boat, and study the problem in a domain which is neither fixed nor a material subdomain, since its evolution is not governed solely by the fluid motion, but also by the motion of the reference frame and by the motion of the stream of water. Nonetheless, it has to comply to the free surface boundary $\Gamma^w(t)$ which is the result of the dynamic boundary condition (1c).

A possible solution is to introduce an intermediate frame of reference, called Arbitrary Lagrangian Eulerian (ALE) (see, for example, [9]). This approach is also known, in the context of potential free surface flows, as the *semi-Lagrangian* approach [5, 21].

2.1. Arbitrary Lagrangian Eulerian Formulation

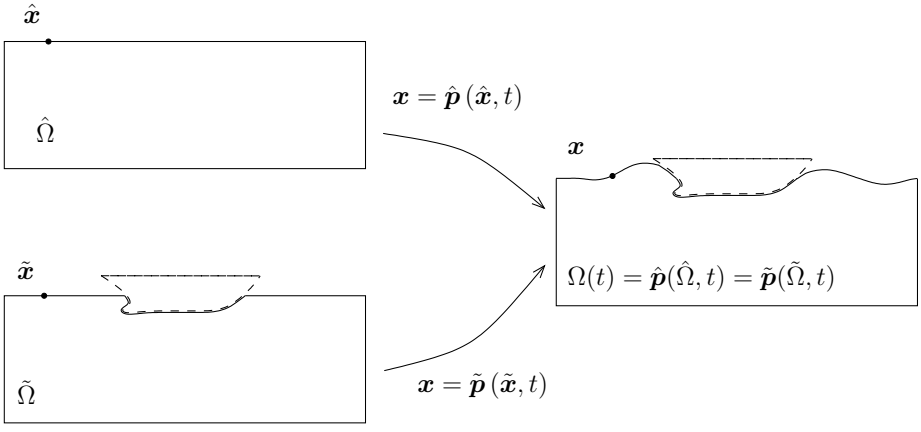

Figure 1: Schematic representation of a Lagrangian motion and of an arbitrary Lagrangian Eulerian motion.

A *motion* is a time parametrized family of invertible maps which associates to each point $\hat{\boldsymbol{x}}$ in a reference domain $\hat{\Omega}$ its position in space at time t:

$$\hat{\boldsymbol{p}} : \hat{\Omega} \times \mathbb{R} \mapsto \mathbb{R}^3, \qquad (\hat{\boldsymbol{x}}, t) \mapsto \boldsymbol{x} = \hat{\boldsymbol{p}}(\hat{\boldsymbol{x}}, t). \tag{4}$$

The domain $\Omega(t)$ at the current time can be seen as the image under the motion $\hat{\boldsymbol{p}}$ of a reference domain $\hat{\Omega}$, i.e., $\hat{\boldsymbol{p}}(\hat{\Omega}, t) = \Omega(t)$. We will indicate with the $\hat{\cdot}$ symbol a *material motion*, or a motion in which the points $\hat{\boldsymbol{x}}$ label material particles.

If one does not want to follow material particles with the domain $\Omega(t)$, it is possible to introduce another intermediate motion, called the *ALE motion*, with which we represent deformations of the domain $\Omega(t)$:

$$\tilde{\boldsymbol{p}} : \tilde{\Omega} \times \mathbb{R} \mapsto \mathbb{R}^3, \qquad (\tilde{\boldsymbol{x}}, t) \mapsto \boldsymbol{x} = \tilde{\boldsymbol{p}}(\tilde{\boldsymbol{x}}, t). \tag{5}$$

These motions can be rather arbitrary, as long as the *shape* of the domain $\Omega(t)$ is preserved by the motion itself, i.e., $\tilde{\boldsymbol{p}}(\tilde{\Omega}, t) = \Omega(t)$. The points labelled with $\tilde{\boldsymbol{x}}$ do not, in general, represent material particles. See Figure 1 for a schematic representation of a Lagrangian motion and of an ALE motion.

Given a Lagrangian field $\hat{q} : \hat{\Omega} \times \mathbb{R} \mapsto \mathbb{R}$, its Eulerian representation is

$$q(\boldsymbol{x}, t) := \hat{q}(\hat{\boldsymbol{p}}^{-1}(\boldsymbol{x}, t), t), \qquad \forall \boldsymbol{x} \in \Omega(t),$$

while, given an Eulerian field $q : \Omega(t) \times \mathbb{R} \mapsto \mathbb{R}$, its Lagrangian representation would be

$$\hat{q}(\hat{\boldsymbol{x}}, t) := q(\hat{\boldsymbol{p}}(\hat{\boldsymbol{x}}, t), t), \qquad \forall \hat{\boldsymbol{x}} \in \hat{\Omega}.$$

A similar structure is valid for ALE fields:

$$\begin{aligned} q(\boldsymbol{x}, t) &:= \tilde{q}(\tilde{\boldsymbol{p}}^{-1}(\boldsymbol{x}, t), t), \qquad \forall \boldsymbol{x} \in \Omega(t), \\ \tilde{q}(\tilde{\boldsymbol{x}}, t) &:= q(\tilde{\boldsymbol{p}}(\tilde{\boldsymbol{x}}, t), t), \qquad \forall \tilde{\boldsymbol{x}} \in \tilde{\Omega}. \end{aligned}$$

The fluid particle velocity $\boldsymbol{v}$ which appears in Problem (1) is the Eulerian representation of the particles velocity

$$\boldsymbol{v}(\hat{\boldsymbol{p}}(\hat{\boldsymbol{x}}, t), t) = \hat{\boldsymbol{v}}(\hat{\boldsymbol{x}}, t) := \frac{\partial \hat{\boldsymbol{p}}(\hat{\boldsymbol{x}}, t)}{\partial t}.$$

In a similar way, we define the Eulerian representation of the *domain velocity*, or *ALE velocity* the field $\boldsymbol{w}$ such that

$$\boldsymbol{w}(\tilde{\boldsymbol{p}}(\tilde{\boldsymbol{x}}, t), t) = \hat{\boldsymbol{w}}(\tilde{\boldsymbol{x}}, t) := \frac{\partial \tilde{\boldsymbol{p}}(\tilde{\boldsymbol{x}}, t)}{\partial t}.$$

Time variations of physical quantities associated with material particles are computed at fixed $\hat{\boldsymbol{x}}$, generating the usual material derivative

$$\frac{Dq(\boldsymbol{x}, t)}{Dt} := \left.\frac{\partial q(\hat{\boldsymbol{p}}(\hat{\boldsymbol{x}}, t), t)}{\partial t}\right|_{\hat{\boldsymbol{x}} = \hat{\boldsymbol{p}}^{-1}(\boldsymbol{x}, t)} = \frac{\partial q(\boldsymbol{x}, t)}{\partial t} + \boldsymbol{v} \cdot \boldsymbol{\nabla} q(\boldsymbol{x}, t).$$

In a similar fashion, if we compute quantities at fixed ALE point $\tilde{\boldsymbol{x}}$, we obtain the ALE time derivative, wich we will denote as

$$\frac{\delta q(\boldsymbol{x},t)}{\delta t} := \left.\frac{\partial q(\tilde{\boldsymbol{p}}(\tilde{\boldsymbol{x}},t),t)}{\partial t}\right|_{\tilde{\boldsymbol{x}}=\tilde{\boldsymbol{p}}^{-1}(\boldsymbol{x},t)} = \frac{\partial q(\boldsymbol{x},t)}{\partial t} + \boldsymbol{w}\cdot\boldsymbol{\nabla} q(\boldsymbol{x},t).$$

The ALE deformation allows one to define the equations of motions in Problem (1) in terms of the fixed ALE reference domain $\tilde{\Omega}$, while still solving the same physical problem. On the free surface part of the boundary, the ALE motion needs to follow the evolution of the fluid particles in order to maintain the correct shape of the domain $\Omega(t)$, in particular the minimum requirement for the ALE motion on the free surface is given by the *free surface kinematic boundary condition*

$$\boldsymbol{w}\cdot\boldsymbol{n} = \boldsymbol{v}\cdot\boldsymbol{n} \qquad \text{on } \Gamma^w(t), \tag{6}$$

which complements the dynamic boundary condition (1c), and provides an evolution equation for the normal part of the ALE motion on the boundary $\Gamma^w(t)$. In terms of the ALE motion, the above condition reads

$$\frac{\partial \tilde{\boldsymbol{p}}}{\partial t}(\tilde{\boldsymbol{x}},t)\cdot\boldsymbol{n} = \boldsymbol{v}(\tilde{\boldsymbol{p}}(\tilde{\boldsymbol{x}},t),t)\cdot\boldsymbol{n} \qquad \text{on } \Gamma^w(t). \tag{7}$$

Equations (1c) and (6) are usually referred to as the free surface dynamic and kinematic boundary conditions, since they represent the physical condition applied to the free surface (equilibrium of the pressure on the water surface) and its evolution equation (the shape of the free surface follows the velocity field of the flow).

2.2. Perturbation potential and boundary conditions

In the context of moving ship hulls, it is desirable to maintain the frame of reference of the domain $\Omega(t)$ around the region where the boat is moving, i.e., we want to solve Problem (3) in a local frame of reference translating with uniform horizontal speed $\boldsymbol{V}_{\mathrm{f}}(t)$. Similarly, one could be interested in studying the behavior of the ship hull in the presence of an horizontal water stream velocity $\boldsymbol{V}_{\mathrm{s}}(t)$, expressed in a global (earth fixed) reference frame.

Uniform accelerations of the reference frame can be taken into account by incorporating them in the body force term

$$\boldsymbol{\beta}\cdot\boldsymbol{x} = \boldsymbol{a}_{\mathrm{f}}\cdot\boldsymbol{x} + gz, \tag{8}$$

and it is convenient to split the potential Φ into the sum between a mean flow potential (due to the stream velocity and to the frame of reference velocity) and the so called *perturbation potential* ϕ due to the presence of the ship hull, namely

$$\Phi(\boldsymbol{x},t) = \big(\boldsymbol{V}_{\mathrm{s}}(t) - \boldsymbol{V}_{\mathrm{f}}(t)\big)\cdot\boldsymbol{x} + \phi(\boldsymbol{x},t) \tag{9a}$$

$$\boldsymbol{v}(\boldsymbol{x},t) = \boldsymbol{\nabla}\Phi(\boldsymbol{x},t) = \boldsymbol{V}_{\mathrm{s}}(t) - \boldsymbol{V}_{\mathrm{f}}(t) + \boldsymbol{\nabla}\phi(\boldsymbol{x},t) \tag{9b}$$

$$\frac{\partial\Phi}{\partial t}(\boldsymbol{x},t) = \big(\boldsymbol{a}_{\mathrm{s}}(t) - \boldsymbol{a}_{\mathrm{f}}(t)\big)\cdot\boldsymbol{x} + \frac{\partial\phi}{\partial t}(\boldsymbol{x},t). \tag{9c}$$

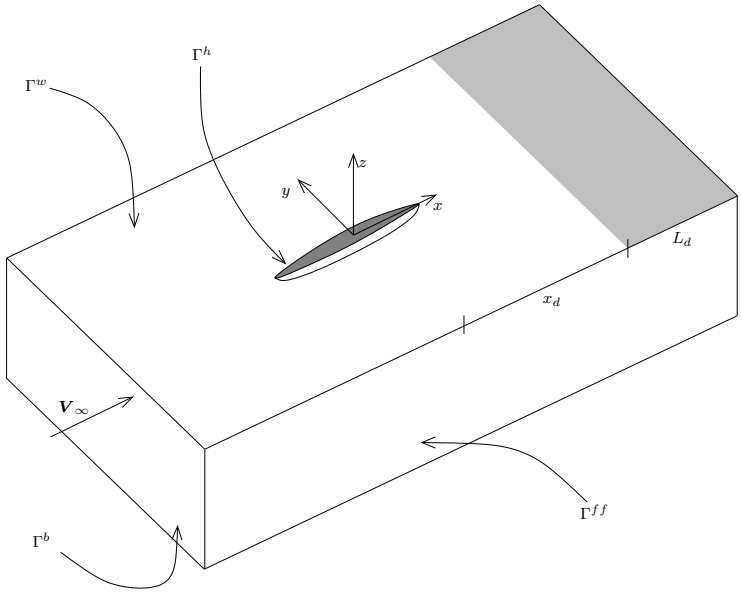

Figure 2: The domain $\Omega(t)$ and the different regions in which its boundary $\partial\Omega(t)$ is split. The grey area behind the hull $\Gamma^h(t)$, is the absorbing beach portion of the free surface region $\Gamma^w(t)$.

The perturbation potential still satisfies Poisson equation

$$\Delta\phi = 0 \qquad \text{in } \Omega(t),$$

and in practice it is convenient to solve for ϕ, and obtain the total potential Φ from equation (9).

In Figure 2 we present a sketch of the domain $\Omega(t)$, with the explicit splitting of the various parts of the boundary $\Gamma(t)$. On the boat hull surface, the non penetration condition takes the form

$$\phi_n := \boldsymbol{\nabla}\phi \cdot \boldsymbol{n} = \boldsymbol{n} \cdot (\boldsymbol{V}_{\mathrm{b}} - \boldsymbol{V}_{\mathrm{s}}) \qquad \text{on } \Gamma^h(t),$$

when expressed in terms of the perturbation potential and $\boldsymbol{V}_{\mathrm{b}}$ is the (given) boat velocity.

On the —horizontal— bottom of the water basin Γ^b, the non penetration condition is also applied, namely

$$\phi_n = 0 \qquad \text{on } \Gamma^b(t).$$

A possible condition for the —vertical— far field boundary is the homogeneous Neumann condition

$$\phi_n = 0 \qquad \text{on } \Gamma^{ff}(t).$$

The most remarkable limit of such condition is the fact that it reflects wave energy back in the computational domain, thus limiting the simulation time. Different boundary conditions can be used to let the wave energy flow outside the domain. We employ an *absorbing beach* technique (see, for example, [7]), in which we add an artificial damping region away from the boat, used to absorb the wave energy. A damping term can be seen as an additional pressure P acting on the free surface. In such case, Bernoulli equation on the free surface becomes

$$\frac{\partial \Phi}{\partial t} + gz - \boldsymbol{a}_{\mathrm{s}} \cdot \boldsymbol{x} + \frac{1}{2}|\boldsymbol{\nabla}\Phi|^2 + \frac{P}{\rho} = 0 \qquad \text{on} \quad \Gamma^w(t), \tag{10}$$

and one can show that the resulting rate of energy absorption is

$$\frac{dE_f}{dt} = \int_{\Gamma^w} P\phi_n \, \mathrm{d}\Gamma. \tag{11}$$

A natural way to construct the damping pressure P is then to use a term which is proportional to the potential normal derivative ϕ_n, which grants a positive energy absorption at all times.

The dynamical free surface boundary condition modified to account for the damping term reads

$$\frac{\partial \Phi}{\partial t} + gz - \boldsymbol{a}_{\mathrm{s}} \cdot \boldsymbol{x} + \frac{1}{2}|\boldsymbol{\nabla}\Phi|^2 - \mu\phi_n = 0 \qquad \text{on} \quad \Gamma^w(t), \tag{12}$$

where

$$\mu = \left(\frac{\max\left(0, x - x_d\right)}{L_d} \right)^2, \tag{13}$$

and x_d is the x coordinate value in which the artificial damping starts to act, while L_d is the length of the absorbing beach, as in Figure 2.

Applying the potential splitting (9) to Problem (3), and summarizing all boundary conditions, we obtain the perturbation potential formulation

$$\Delta\phi = 0 \qquad \text{in } \Omega(t) \tag{14a}$$

$$\frac{\partial \phi}{\partial t} + \boldsymbol{v} \cdot \boldsymbol{\nabla}\phi = -gz + \boldsymbol{a}_{\mathrm{s}} \cdot \boldsymbol{x} + \frac{1}{2}|\boldsymbol{\nabla}\phi|^2 - \mu\phi_n \qquad \text{on } \Gamma^w(t) \tag{14b}$$

$$\phi(\boldsymbol{x}, 0) = \phi_0(\boldsymbol{x}) \qquad \text{on } \Gamma^w(0) \tag{14c}$$

$$\phi_n = \boldsymbol{n} \cdot (\boldsymbol{V}_{\mathrm{b}} - \boldsymbol{V}_{\mathrm{s}}) \qquad \text{on } \Gamma^h(t) \tag{14d}$$

$$\phi_n = 0 \qquad \text{on } \Gamma^b(t) \cup \Gamma^{ff}(t) \tag{14e}$$

$$\boldsymbol{w} \cdot \boldsymbol{n} = \boldsymbol{v} \cdot \boldsymbol{n} \qquad \text{on } \tilde{\Gamma}^w(t), \tag{14f}$$

where $\boldsymbol{v} = \boldsymbol{V}_{\mathrm{s}} - \boldsymbol{V}_{\mathrm{f}} + \boldsymbol{\nabla}\phi$. Equation (14f) is the kinematic boundary condition for the evolution of the free surface parametrization, while Equation (14b) is a dynamic Dirichlet boundary condition for the Poisson problem (14a) at each time t, whose initial condition is given by Equation (14c).

Problem (14) can be rewritten in terms of ALE derivatives as

$$\Delta\phi = 0 \qquad \text{in } \Omega(t) \tag{15a}$$

$$\frac{\delta\phi}{\delta t} + (\boldsymbol{v} - \boldsymbol{w}) \cdot \boldsymbol{\nabla}\phi = -g\eta + \boldsymbol{a}_{\mathrm{s}} \cdot \boldsymbol{x} + \frac{1}{2}|\boldsymbol{\nabla}\phi|^2 - \mu\phi_n \qquad \text{on } \Gamma^w(t) \tag{15b}$$

$$\phi(\boldsymbol{x}, 0) = \phi_0(\boldsymbol{x}) \qquad \text{on } \Gamma^w(0) \tag{15c}$$

$$\phi_n = \boldsymbol{n} \cdot (\boldsymbol{V}_{\mathrm{b}} - \boldsymbol{V}_{\mathrm{s}}) \qquad \text{on } \Gamma^h(t) \tag{15d}$$

$$\phi_n = 0 \qquad \text{on } \Gamma^b(t) \cup \Gamma^{ff}(t) \tag{15e}$$

$$\boldsymbol{w} \cdot \boldsymbol{n} = \boldsymbol{v} \cdot \boldsymbol{n} \qquad \text{on } \Gamma(t), \tag{15f}$$

where we notice that, whenever $\boldsymbol{w} = \boldsymbol{v}$, we recover a fully Lagrangian formulation (the ALE motion is, in this case, following the particles motion and $\delta/\delta t \equiv D/Dt$). Similarly, if the domain is fixed, and we set $\boldsymbol{w} = 0$, we recover the classical Eulerian formulation (14) on fixed domains, and $\delta/\delta t \equiv \partial/\partial t$.

If the free surface can be seen as the graph of a single valued function $\eta(x, y, t)$ of the horizontal components x and y, then

$$\boldsymbol{x} = (x, y, \eta(x, y, t)) \qquad \text{on } \Gamma^w(t), \tag{16}$$

and, for a material particle on the free surface, we have

$$\hat{\boldsymbol{p}}(\hat{\boldsymbol{x}}, t) \cdot \boldsymbol{e}_z = \eta(\hat{\boldsymbol{p}}(\hat{\boldsymbol{x}}, t), t), \tag{17}$$

where we define $\eta(\boldsymbol{x}, t) := \eta(\boldsymbol{x} \cdot \boldsymbol{e}_x, \boldsymbol{x} \cdot \boldsymbol{e}_y, t)$. Taking the time derivative of Equation (17) we get

$$\frac{\partial\hat{\boldsymbol{p}}}{\partial t}(\hat{\boldsymbol{x}}, t) \cdot \boldsymbol{e}_z = \frac{\partial\eta}{\partial t}(\hat{\boldsymbol{p}}(\hat{\boldsymbol{x}}, t), t) + \frac{\partial\hat{\boldsymbol{p}}}{\partial t}(\hat{\boldsymbol{x}}, t) \cdot \boldsymbol{\nabla}\eta(\hat{\boldsymbol{p}}(\hat{\boldsymbol{x}}, t), t) \qquad \text{on } \hat{\Gamma}^w,$$

that is, in Eulerian form:

$$\boldsymbol{v}_z = \frac{\partial\eta}{\partial t} + \boldsymbol{v} \cdot \boldsymbol{\nabla}\eta = \frac{D\eta}{Dt} \qquad \text{on } \Gamma^w(t), \tag{18}$$

where $\partial\eta/\partial z \equiv 0$. Proceeding in the same way for the ALE deformation and the ALE velocity of the domain, we get

$$\boldsymbol{w}_z = \frac{\partial\eta}{\partial t} + \boldsymbol{w} \cdot \boldsymbol{\nabla}\eta = \frac{\delta\eta}{\delta t} \qquad \text{on } \Gamma^w(t). \tag{19}$$

Isolating $\partial\eta/\partial t$ in Equation (18) and substituting in Equation (19), we get an alternative expression for Condition (15f)[1],

$$\frac{\delta\eta}{\delta t} + (\boldsymbol{v} - \boldsymbol{w}) \cdot \boldsymbol{\nabla}\eta = \boldsymbol{v} \cdot \boldsymbol{e}_z \qquad \text{on } \Gamma^w(t), \tag{20}$$

[1]That conditions (15f) and (20) are equivalent in this framework, comes immediately from the observation that, when $\Gamma^w(t)$ is the graph of the function $\eta(x, y, t)$, then the normal to the surface $\Gamma^w(t)$ itself is given by a vector proportional to $\boldsymbol{e}_z - \boldsymbol{\nabla}\eta$. Substituting in Equation (15f) gives immediately Equation (20).

which is valid for nonbreaking waves in which $\eta(x, y, t)$ is single-valued.

Equation (20) is the kinematic boundary condition for the evolution of the unknown free surface elevation $\eta(x, y, t)$ which is often found in the literature of semi-Lagrangian methods for potential free surface flows [4, 5, 21].

Equation (20) is rather general, and is valid for *arbitrary* values of horizontal ALE velocities. Suitable values of $\boldsymbol{V}_{\mathrm{s}}$ and $\boldsymbol{V}_{\mathrm{f}}$ can be plugged into the velocity field $\boldsymbol{v} = (\boldsymbol{V}_{\mathrm{s}} - \boldsymbol{V}_{\mathrm{f}} + \boldsymbol{\nabla}\phi)$ to specify them for the desired reference frame. For instance, setting $\boldsymbol{V}_{\mathrm{s}} = \boldsymbol{V}_{\mathrm{f}} = 0$, and $\boldsymbol{w} = \left(0, 0, \frac{\delta\eta}{\delta t}\right)$, one obtains

$$\begin{aligned}
\frac{\delta\eta}{\delta t} &= \frac{\partial\phi}{\partial z} + \boldsymbol{\nabla}\eta \cdot (\boldsymbol{w} - \boldsymbol{\nabla}\phi) = \frac{\partial\phi}{\partial z} - \frac{\partial\phi}{\partial x}\frac{\partial\eta}{\partial x} - \frac{\partial\phi}{\partial y}\frac{\partial\eta}{\partial y} \\
\frac{\delta\phi}{\delta t} &= -g\eta + \frac{1}{2}|\boldsymbol{\nabla}\phi|^2 + \boldsymbol{\nabla}\phi \cdot (\boldsymbol{w} - \boldsymbol{\nabla}\phi) = -g\eta + \frac{\partial\phi}{\partial z}\frac{\delta\eta}{\delta t},
\end{aligned}$$

which are the semi-Lagrangian equations written in an earth fixed reference frame, and null stream velocity used in [17].

In this work, we choose instead to solve the problem in a coordinate system attached to the ship hull. We move the reference frame according to the horizontal average velocity of the boat, that is we set $\boldsymbol{V}_{\mathrm{f}} = (\overline{\boldsymbol{V}}_{\mathrm{b}} \cdot \boldsymbol{e}_x)\boldsymbol{e}_x =: -\boldsymbol{V}_\infty = (-V_\infty, 0, 0)$ and we assume $\boldsymbol{V}_{\mathrm{s}} = 0$. With these values, Equations (20) and (15b) take the form

$$\frac{\delta\eta}{\delta t} = \frac{\partial\phi}{\partial z} + \boldsymbol{\nabla}\eta \cdot (\boldsymbol{w} - \boldsymbol{\nabla}\phi - \boldsymbol{V}_\infty) \tag{21}$$

$$\frac{\delta\phi}{\delta t} = -g\eta + \frac{1}{2}|\boldsymbol{\nabla}\phi|^2 + \boldsymbol{\nabla}\phi \cdot (\boldsymbol{w} - \boldsymbol{\nabla}\phi - \boldsymbol{V}_\infty) - \mu\phi_n, \tag{22}$$

which coincide with the ones proposed by Beck *et al.* [5], and in which the points on the free surface move with an a priori arbitrary horizontal speed in the boat reference frame.

2.3. Boundary integral formulation

While Equation (15a) is time dependent and defined in the entire domain $\Omega(t)$, we are really only interested in its solution on the boundary $\Gamma(t)$, in particular on the unknown free surface part of the boundary, and on the ship hull, where we would like to recover the pressure distribution by postprocessing Bernoulli's equation (3a).

At any given time instant $\bar{t}$ we want to compute ϕ satisfying

$$-\Delta\phi = 0 \qquad \text{in } \Omega(\bar{t}) \tag{23a}$$

$$\phi = \overline{\phi} \qquad \text{on } \Gamma^w(\bar{t}) \tag{23b}$$

$$\phi_n = \overline{\phi_n} \qquad \text{on } \Gamma^h(\bar{t}) \cup \Gamma^b(\bar{t}) \cup \Gamma^{ff}(\bar{t}) \tag{23c}$$

where $\overline{\phi}$ is the potential on the free surface at the time $\bar{t}$, and $\overline{\phi_n}$ is equal to zero on $\Gamma^b(\bar{t}) \cup \Gamma^{ff}(\bar{t})$ and to $\left(\boldsymbol{V}_{\mathrm{b}}(\bar{t}) - \boldsymbol{V}_\infty(\bar{t})\right) \cdot \boldsymbol{n}$ on $\Gamma^h(\bar{t})$.

This is a purely spatial boundary value problem, in which time appears only through boundary conditions and through the shape of the time dependent domain.

The solution of this boundary value problem allows the computation of the full potential gradient on the boundary $\Gamma(t)$, which is what is required in the dynamic and kinematic boundary conditions to advance the time evolution of both ϕ and η.

Using the second Green identity

$$\int_\Omega (-\Delta u) v \, dx + \int_{\partial\Omega} \frac{\partial u}{\partial n} v \, \mathrm{d}s = \int_\Omega (-\Delta v) u \, dx + \int_{\partial\Omega} \frac{\partial v}{\partial n} u \, \mathrm{d}s,$$

a solution to system (23) can be expressed in terms of a boundary integral representation only, via convolutions with fundamental solutions of the Laplace problem.

We call G the *free space Green's function*, i.e., the function

$$G(\boldsymbol{r}) = \frac{1}{4\pi|\boldsymbol{r}|},$$

which is the distributional solution of

$$\begin{aligned} &-\Delta G(\boldsymbol{x} - \boldsymbol{x}_0) = \delta(\boldsymbol{x}_0) && \text{in } \mathbb{R}^3 \\ &\lim_{|\boldsymbol{x}|\to\infty} G(\boldsymbol{x} - \boldsymbol{x}_0) = 0, \end{aligned} \tag{24}$$

where $\delta(\boldsymbol{x}_0)$ is the Dirac distribution centered in $\boldsymbol{x}_0$.

If we select $\boldsymbol{x}_0$ to be inside $\Omega(t)$, use the defining property of the Dirac delta and the second Green identity, we obtain

$$\begin{aligned} \phi(\boldsymbol{x}_0, t) = \int_{\Omega(t)} \left[- \left(\Delta G(\boldsymbol{x} - \boldsymbol{x}_0) \right) \phi(\boldsymbol{x}, t) \right] \mathrm{d}\Omega = \\ \int_{\Gamma(t)} \left[(\boldsymbol{\nabla}\phi(\boldsymbol{x}, t) \cdot \boldsymbol{n}) G(\boldsymbol{x} - \boldsymbol{x}_0) - (\boldsymbol{\nabla} G(\boldsymbol{x} - \boldsymbol{x}_0) \cdot \boldsymbol{n}) \phi(\boldsymbol{x}, t) \right] \mathrm{d}\Gamma. \end{aligned}$$

In the limit for $\boldsymbol{x}_0$ touching the boundary $\Gamma(t)$, the integral on the right hand side will have a singular argument, and should be evualated according to the Cauchy principal value. This process yields the so called *Boundary Integral Equation* (BIE)

$$\alpha\phi = \int_{\Gamma(t)} \left[\phi_n G - \frac{\partial G}{\partial n} \phi \right] \mathrm{d}\Gamma \qquad \text{on } \Gamma(t), \tag{25}$$

where $\alpha(\boldsymbol{x}, t)$ is the fraction of solid angle 4π with which the domain $\Omega(t)$ is seen from $\boldsymbol{x}$ and the gradient of the free space Green's function is given by

$$\boldsymbol{\nabla} G(\boldsymbol{r}) \cdot \boldsymbol{n} = -\frac{\boldsymbol{r} \cdot \boldsymbol{n}}{4\pi \left|\boldsymbol{r}\right|^3}.$$

The function $\alpha(\boldsymbol{x}, t)$ can be computed by noting that the constant function 1 is a solution to the Laplace equation with zero normal derivative, and therefore it must be

$$\alpha = -\int_{\Gamma(t)} \frac{\partial G}{\partial n} d\Gamma \qquad \text{on } \Gamma(t), \tag{26}$$

in the Cauchy principal value sense.

With Equation (25), the continuity equation has been reformulated as a boundary integral equation of mixed type defined on the moving boundary $\Gamma(t)$, where the main ingredients are the perturbation potential $\phi(\boldsymbol{x}, t)$ and its normal derivative $\phi_n(\boldsymbol{x}, t)$.

The domain deformation $\boldsymbol{p}(\boldsymbol{x}, t)$ on the free surface takes the form

$$\boldsymbol{p}(\boldsymbol{x}, t) = (x, y, \eta(x, y, t)) \qquad \text{on } \Gamma^w(t), \tag{27}$$

and one has to solve an additional boundary value problem to uniquely determine the full ALE motion $\tilde{\boldsymbol{p}}(\tilde{\boldsymbol{x}}, t)$.

2.4. Arbitrary Lagrangian Eulerian motion

When the arbitrary Lagrangian Eulerian formulation is used in the finite element framework (see, for example, [9]), the restriction to the boundary $\Gamma(t)$ of the deformation $\tilde{\boldsymbol{p}}(\tilde{\boldsymbol{x}}, t)$ is either known, or entirely determined by the equations of motion. In this case, an additional boundary value problem needs to be solved to recover the domain deformation in the interior of $\Omega(t)$ starting from the Dirichlet values on the boundary.

Our situation is slightly different, since only the *normal* component of the motion is given on the boundary $\Gamma(t)$, and we are not really interested in finding a domain motion in the interior of $\Omega(t)$.

In the dynamic and kinematic boundary conditions (21) and (22) we have the freedom to choose an ALE motion arbitrarily, as long as the shape of $\Gamma(t)$ is preserved. In analogy to what is done in the finite element framework, we construct an additional boundary value problem to determine uniquely $\tilde{\boldsymbol{p}}(\tilde{\boldsymbol{x}}, t)$.

A typical choice in the finite element framework is based on linear elasticity theory, and requires the solution of an additional Laplace problem on the coordinates $\tilde{\boldsymbol{p}}(\tilde{\boldsymbol{x}}, t)$, or, in some cases, a bi-Laplacian. This procedure can be generalized to surfaces embedded in three-dimensional space via the Laplace-Beltrami operator.

The Laplace-Beltrami operator can be constructed from the surface gradient $\boldsymbol{\nabla}_s g(\boldsymbol{x}, t)$, defined as

$$\boldsymbol{\nabla}_s a(\boldsymbol{x}, t) := \boldsymbol{\nabla} \overline{a} - (\boldsymbol{\nabla} \overline{a} \cdot \boldsymbol{n}) \boldsymbol{n}, \qquad \forall \overline{a} \text{ s.t. } \overline{a} = a(\boldsymbol{x}, t) \quad \text{on } \Gamma(t), \tag{28}$$

where $\overline{a}$ is an arbitrary smooth extension of $a(\boldsymbol{x}, t)$ on a tubular neighborhood of $\Gamma(t)$. Definition (28) is independent on the extension used (see, for example, [8]). Similarly, we indicate with $\tilde{\boldsymbol{\nabla}}_s$ the surface gradient computed in the reference domain $\tilde{\Gamma}$, with the same definition as in (28), but replacing $\boldsymbol{x}$ with $\tilde{\boldsymbol{x}}$, and performing all differential operators in terms of the independent variable $\tilde{\boldsymbol{x}}$ instead of $\boldsymbol{x}$.

If we indicate with $\boldsymbol{\nabla}_s \cdot$ the surface divergence (i.e., the trace of the surface gradient $\boldsymbol{\nabla}_s$), then the surface Laplacian Δ_s and $\tilde{\Delta}_s$ on $\Gamma(t)$ and on $\tilde{\Gamma}$, are given by $\Delta_s := \boldsymbol{\nabla}_s \cdot \boldsymbol{\nabla}_s$, and by $\tilde{\Delta}_s := \tilde{\boldsymbol{\nabla}}_s \cdot \tilde{\boldsymbol{\nabla}}_s$.

We use the shorthand notation $\gamma^{a,b}(t)$ to indicate the intersection between $\Gamma^a(t)$ and $\Gamma^b(t)$, that is,

$$\gamma^{a,b}(t) = \overline{\Gamma^a(t)} \cap \overline{\Gamma^b(t)} \qquad a \neq b,$$

where a, b are either w, h, b or ff. We indicate with $\gamma(t)$ the union of all curves $\gamma^{a,b}(t)$.

The curve $\gamma^{w,h}(t)$ is usually referred to as the *waterline* on the hull of the ship. On $\gamma^{w,h}(t)$, the domain velocity $\boldsymbol{w}$ has to satisfy the kinematic boundary condition for *both* the free surface and the ship hull:

$$\begin{aligned} \boldsymbol{w} \cdot \boldsymbol{n}^w &= \boldsymbol{v} \cdot \boldsymbol{n}^w && \text{on } \gamma^{w,h}(t) \\ \boldsymbol{w} \cdot \boldsymbol{n}^h &= 0 && \text{on } \gamma^{w,h}(t), \end{aligned} \tag{29}$$

where $\boldsymbol{n}^w$ is the normal to the free surface and $\boldsymbol{n}^h$ is the normal to the hull surface. When both conditions are enforced, $\boldsymbol{w}$ is still allowed to be arbitrary along the direction tangent to the waterline.

There are several options to select the tangent velocity $\boldsymbol{w}_t$ defined as

$$\boldsymbol{w}_t := \boldsymbol{w} \cdot (\boldsymbol{n}^h \times \boldsymbol{n}^w) = \boldsymbol{w} \cdot \boldsymbol{t}.$$

A natural possibility is to choose zero tangential velocity. Other choices are certainly possible, and may be preferable, for example, if one would like to cluster computational nodes in regions where the curvature of the waterline is higher. In the experiments we present, the tangential velocity is always set to zero.

Conditions (29) and zero tangential velocity, uniquely determine an evolution equation for the ALE deformation on $\tilde{\gamma}^{w,h}$. Here we summarize all boundary conditions for the evolution of $\tilde{\boldsymbol{p}}(\tilde{\boldsymbol{x}}, t)$ on the entire $\tilde{\gamma}$:

$$\begin{aligned} \boldsymbol{w} \cdot \boldsymbol{n}^w &= \boldsymbol{v} \cdot \boldsymbol{n}^w && \text{on } \gamma^{w,h}(t) \\ \boldsymbol{w} \cdot \boldsymbol{n}^h &= 0 && \text{on } \gamma^{w,h}(t) \\ \boldsymbol{w} \cdot (\boldsymbol{n}^h \times \boldsymbol{n}^w) &= 0 && \text{on } \gamma^{w,h}(t) \end{aligned} \tag{30a}$$

$$\begin{aligned} \boldsymbol{w} \cdot \boldsymbol{n}^w &= \boldsymbol{v} \cdot \boldsymbol{n}^w && \text{on } \gamma^{w,ff}(t) \\ \boldsymbol{w} \cdot \boldsymbol{n}^{ff} &= 0 && \text{on } \gamma^{w,ff}(t) \\ \boldsymbol{w} \cdot (\boldsymbol{n}^w \times \boldsymbol{n}^{ff}) &= 0 && \text{on } \gamma^{w,ff}(t) \end{aligned} \tag{30b}$$

$$\boldsymbol{w} = 0 \qquad \text{on } \gamma^{b,ff}(t). \tag{30c}$$

Expressing the boundary conditions (30) as a given velocity term $\boldsymbol{w}_g$, the evolution equation of $\gamma(t)$ become

$$\begin{aligned} \frac{\partial \tilde{\boldsymbol{p}}_\gamma}{\partial t}(\tilde{\boldsymbol{x}}, t) &= \boldsymbol{w}_g(\tilde{\boldsymbol{p}}_\gamma(\tilde{\boldsymbol{x}}, t)) && \text{on } \tilde{\gamma} \\ \tilde{\boldsymbol{p}}_\gamma(\tilde{\boldsymbol{x}}, 0) &= \tilde{\boldsymbol{p}}_0(\tilde{\boldsymbol{x}}) && \text{on } \tilde{\gamma}. \end{aligned} \tag{31}$$

A reconstruction of a reasonable ALE deformation on the entire $\Gamma(t)$ is then possible by solving an additional elliptic boundary value problem, coupled with a projection on the surface of the ship hull and on the free surface. Given a free surface configuration η and the deformation $\tilde{\boldsymbol{p}}_\gamma$ on the wireframe $\tilde{\gamma}$, in order to find a compatible deformation $\tilde{\boldsymbol{p}}$ on the entire $\tilde{\Gamma}$, we solve the additional problem

$$\begin{aligned} -\tilde{\Delta}_s \tilde{\boldsymbol{g}} &= -2\tilde{\boldsymbol{n}}\tilde{k} && \text{on } \tilde{\Gamma} \\ \tilde{\boldsymbol{g}} &= \tilde{\boldsymbol{p}}_\gamma && \text{on } \tilde{\gamma} \\ \\ \tilde{\boldsymbol{p}} &= \mathcal{P}_h\, \tilde{\boldsymbol{g}} && \text{on } \tilde{\Gamma}^h \\ \tilde{\boldsymbol{p}} &= \mathcal{P}_\eta\, \tilde{\boldsymbol{g}} := \tilde{\boldsymbol{g}} + (\eta(\tilde{\boldsymbol{g}}) - \tilde{\boldsymbol{g}} \cdot \boldsymbol{e}_z)\boldsymbol{e}_z && \text{on } \tilde{\Gamma}^w \\ \\ \tilde{\boldsymbol{p}} &= \tilde{\boldsymbol{g}} && \text{on } \tilde{\Gamma}^b \cup \tilde{\Gamma}^{ff}, \end{aligned} \tag{32}$$

where $\tilde{k}(\tilde{\boldsymbol{x}})$ is the mean curvature of the domain $\tilde{\Gamma}$, i.e., the mean curvature of the hull on $\tilde{\Gamma}^h$ and zero eveywhere else, while $\mathcal{P}_h$ is a projection operator on the hull surface. Similarly, $\mathcal{P}_\eta$ is a (vertical) projection operator on the free surface.

The auxiliary function $\tilde{\boldsymbol{g}}$ represents a surface that follows the waterline deformation $\tilde{\boldsymbol{p}}_\gamma$. On the ship hull, it is a perturbation of the shape of the hull while everywhere else it is a minimal surface with boundary conditions imposed by $\tilde{\boldsymbol{p}}_\gamma$. On the free surface, only its x and y components are used to determine $\tilde{\boldsymbol{p}}$, while η (which satisfies the kinematic boundary conditions (20)) imposes the z component.

2.5. Integro-differential formulation

Putting everything together, the final integro-differential system is given by the following problem:

Given initial conditions ϕ_0 and η_0 on $\Gamma^w(0)$, and $\tilde{\boldsymbol{p}}_0$ on $\tilde{\gamma}$, for each time

$t \in [0, T]$, find $\tilde{\boldsymbol{p}}$, ϕ, ϕ_n that satisfy

$$\int_{\Gamma(t)} \frac{\partial G}{\partial n} \phi \, \mathrm{d}\Gamma - \phi \int_{\Gamma(t)} \frac{\partial G}{\partial n} \, \mathrm{d}\Gamma = \int_{\Gamma(t)} \phi_n G \, \mathrm{d}\Gamma \qquad \text{on } \Gamma(t) \tag{33a}$$

$$\frac{\delta \phi}{\delta t} = V_\phi(\phi, \phi_n, \eta, \boldsymbol{w}) \qquad \text{on } \Gamma^w(t) \tag{33b}$$

$$\frac{\delta \eta}{\delta t} = V_\eta(\phi, \phi_n, \eta, \boldsymbol{w}) \qquad \text{on } \Gamma^w(t) \tag{33c}$$

$$\phi(\boldsymbol{x}, 0) = \phi_0(\boldsymbol{x}) \qquad \text{on } \Gamma^w(0) \tag{33d}$$

$$\eta(\boldsymbol{x}, 0) = \eta_0(\boldsymbol{x}) \qquad \text{on } \Gamma^w(0) \tag{33e}$$

$$\phi_n = \overline{\phi_n} \qquad \text{on } \Gamma^N(t) \tag{33f}$$

$$\boldsymbol{w} \cdot \boldsymbol{n} = 0 \qquad \text{on } \Gamma^N(t) \tag{33g}$$

$$-\tilde{\Delta}_s \tilde{\boldsymbol{g}} = -2\tilde{\boldsymbol{n}} k \qquad \text{on } \tilde{\Gamma} \setminus \tilde{\gamma} \tag{33h}$$

$$\frac{\partial \tilde{\boldsymbol{g}}_\gamma}{\partial t}(\tilde{\boldsymbol{x}}, t) = \boldsymbol{w}_g(\tilde{\boldsymbol{g}}(\tilde{\boldsymbol{x}}, t)) \qquad \text{on } \tilde{\gamma} \tag{33i}$$

$$\tilde{\boldsymbol{p}}(\tilde{\boldsymbol{g}}, 0) = \tilde{\boldsymbol{p}}_0(\tilde{\boldsymbol{g}}) \qquad \text{on } \tilde{\gamma} \tag{33j}$$

$$\tilde{\boldsymbol{p}} = \mathcal{P}\, \tilde{\boldsymbol{g}} \qquad \text{on } \tilde{\Gamma}. \tag{33k}$$

where we used the shorthand notations

$$\boldsymbol{w} := \frac{\delta \boldsymbol{p}}{\delta t} \tag{34a}$$

$$\boldsymbol{v} := \boldsymbol{V}_\infty - \boldsymbol{V}_\mathrm{f} + \boldsymbol{\nabla} \phi \tag{34b}$$

$$V_\phi(\phi, \phi_n, \eta, \boldsymbol{w}) := (\boldsymbol{w} - \boldsymbol{v}) \cdot \boldsymbol{\nabla} \phi - g\eta + \boldsymbol{a}_\infty \cdot \boldsymbol{x} + \frac{1}{2} |\boldsymbol{\nabla} \phi|^2 - \mu \phi_n \tag{34c}$$

$$V_\eta(\phi, \phi_n, \eta, \boldsymbol{w}) := (\boldsymbol{w} - \boldsymbol{v}) \cdot \boldsymbol{\nabla} \eta + \boldsymbol{v} \cdot \boldsymbol{e}_z \tag{34d}$$

$$\Gamma^N(t) := \Gamma^h(t) \cup \Gamma^b(t) \cup \Gamma^{ff}(t) \tag{34e}$$

$$\overline{\phi_n} := \begin{cases} (\boldsymbol{V}_\mathrm{b} - \boldsymbol{V}_\mathrm{f}) \cdot \boldsymbol{n} & \text{on } \Gamma^h(t) \\ 0 & \text{on } \Gamma^b(t) \cup \Gamma^{ff}(t), \end{cases} \tag{34f}$$

$$\mathcal{P}\tilde{\boldsymbol{g}} := \begin{cases} \mathcal{P}_h\, \tilde{\boldsymbol{g}} & \text{on } \tilde{\Gamma}^h \\ \mathcal{P}_\eta\, \tilde{\boldsymbol{g}} := \tilde{\boldsymbol{g}} + (\eta(\tilde{\boldsymbol{g}}, t) - \tilde{\boldsymbol{g}} \cdot \boldsymbol{e}_z) \boldsymbol{e}_z & \text{on } \tilde{\Gamma}^w \\ \tilde{\boldsymbol{g}} & \text{on } \tilde{\Gamma}^b \cup \tilde{\Gamma}^{ff}, \end{cases} \tag{34g}$$

and both the potential and the pressure in the entire domain can be obtained by postprocessing the solution to Problem (33) with the boundary integral representation (24) and with Bernoulli's Equation (3a).

The full gradient of the perturbation potential on the surface $\Gamma(t)$ that appears in Equations (34b), (34c) and (34d) is constructed from the surface gradient of ϕ and from the normal gradient ϕ_n as

$$\boldsymbol{\nabla} \phi(\boldsymbol{x}, t) := \boldsymbol{\nabla}_s \phi(\boldsymbol{x}, t) + \phi_n(\boldsymbol{x}, t) \boldsymbol{n}.$$

A numerical discretization of the continuous Problem (33) is done on the *fixed* boundary $\tilde{\Gamma}$ of the reference domain $\tilde{\Omega}$, with independent variable $\tilde{\boldsymbol{x}}$ which will label node locations in a reference computational grid, and the motion $\tilde{\boldsymbol{p}}(\tilde{\boldsymbol{x}}, t)$ will denote the trajectory of the computational nodes.

3. Numerical discretization

To approximate the continuous problem, we introduce a decomposition $\tilde{\Gamma}_h$ for $\tilde{\Gamma}$ made of quadrilaterals in three dimensional space, such that the usual regularity assumptions are satisfied:

1. $\overline{\tilde{\Gamma}} = \cup\{K \in \tilde{\Gamma}_h\}$;
2. Any two cells K, K' only intersect in common faces, edges, or vertices;
3. The decompositions $\tilde{\Gamma}_h$ matches the decomposition $\tilde{\Gamma} = \tilde{\Gamma}^w \cup \tilde{\Gamma}^h \cup \tilde{\Gamma}^b \cup \tilde{\Gamma}^{ff}$.

On the decomposition $\tilde{\Gamma}_h$, we look for solutions $(\boldsymbol{p}_h, \phi_h, \phi_{nh})$ in the finite dimensional spaces Y_h, V_h, and Q_h defined as

$$Y_h := \left\{ \boldsymbol{u}_h \in \mathcal{C}^0(\tilde{\Gamma}_h)^3 \,\middle|\, \boldsymbol{u}_{h|K} \in \mathcal{P}_Y(K)^3,\, K \in \tilde{\Gamma}_h \right\} \equiv \operatorname{span}\{\boldsymbol{v}_h^i\}_{i=1}^{N_Y} \tag{35}$$

$$V_h := \left\{ \phi_h \in \mathcal{C}^0(\tilde{\Gamma}_h) \;\middle|\, \phi_{h|K} \in \mathcal{P}_V(K),\, K \in \tilde{\Gamma}_h \right\} \equiv \operatorname{span}\{\varphi_h^i\}_{i=1}^{N_V} \tag{36}$$

$$Q_h := \left\{ \gamma_h \in \mathcal{C}^0(\tilde{\Gamma}_h) \;\middle|\, \gamma_{h|K} \in \mathcal{P}_Q(K),\, K \in \tilde{\Gamma}_h \right\} \equiv \operatorname{span}\{\tau_h^i\}_{i=1}^{N_Q}, \tag{37}$$

where $\mathcal{P}_Y(K)$, $\mathcal{P}_V(K)$ and $\mathcal{P}_Q(K)$ are polynomial spaces of degree r_Y, r_V and r_Q respectively on the cells K, and N_Y, N_V and N_Q are the dimensions of each finite dimensional space.

The most common approach for the solution of the boundary integral equation (25) in the engineering community is the *collocation boundary element method*, where the continuous functions ϕ and $\boldsymbol{\nabla}\phi \cdot \boldsymbol{n}$ are replaced by their discrete counterparts and the boundary integral equation is imposed at a sufficient number of points on $\Gamma(t)$.

Once a geometric representation of the reference domain $\tilde{\Gamma}_h$ is available as a collection of quadrilaterals K, we could in principle choose arbitrary discretizations of the functional spaces V_h, Q_h and Y_h, which may not be related with the geometrical discretization. A more natural choice, however, is given by the *iso-parametric* representation, where the shape of the deformed surface $\Gamma_h(t)$, i.e., the map $\tilde{\boldsymbol{p}}(\tilde{\boldsymbol{x}}, t)$, the surface potential $\phi_h(\boldsymbol{x}, t)$ and its normal derivative $\phi_n(\boldsymbol{x}, t)$ on the k-th panel are based on the same parametrization used for the panel geometry, that is, we choose

$$Q_h = V_h, \qquad Y_h = V_h^3 = \operatorname{span}\{\varphi_h^i \boldsymbol{e}_x, \varphi_h^i \boldsymbol{e}_y, \varphi_h^i \boldsymbol{e}_z\}_{i=1}^{N_V}. \tag{38}$$

We indicate with the notation $\{\phi\}$ and $\{\phi_n\}$ the column vectors of time dependent coefficients $\phi^i(t)$ and ${\phi_n}^j(t)$ such that

$$\begin{aligned} \phi_h(\boldsymbol{x},t) &:= \sum_{i=1}^{N_V} \phi^i(t)\varphi_h^i(\tilde{\boldsymbol{p}}_h^{-1}(\boldsymbol{x},t)) \qquad \text{on } \Gamma_h(t) \\ \phi_{nh}(\boldsymbol{x},t) &:= \sum_{j=1}^{N_V} {\phi_n}^j(t)\varphi_h^j(\tilde{\boldsymbol{p}}_h^{-1}(\boldsymbol{x},t)) \qquad \text{on } \Gamma_h(t), \end{aligned} \tag{39}$$

where the map $\tilde{\boldsymbol{p}}_h^{-1}(\boldsymbol{x},t)$ is the inverse of the ALE deformation

$$\tilde{\boldsymbol{p}}_h(\tilde{\boldsymbol{x}},t) := \sum_{k=0}^{N_V} \boldsymbol{x}^k(t)\varphi_h^k(\tilde{\boldsymbol{x}}) \qquad \text{on } \tilde{\Gamma}, \tag{40}$$

and $\boldsymbol{x}^k$ represents the current location of the vertices or control points that define the current configuration of $\Gamma(t)$.

To distinguish matrices from column vectors, we will indicate matrices with the bracket notation, e.g.., $[M]$. The ALE derivatives of the finite dimensional $\phi_h(\boldsymbol{x},t)$ and $\boldsymbol{p}_h(\boldsymbol{x},t)$ can be expressed as

$$\begin{aligned} \frac{\delta\phi_h}{\delta t}(\boldsymbol{x},t) &= \sum_{i=1}^{N_V} \frac{\partial\phi^i}{\partial t}(t)\varphi_h^i(\tilde{\boldsymbol{p}}_h^{-1}(\boldsymbol{x},t)) \\ \boldsymbol{w}_h(\boldsymbol{x},t) := \frac{\delta\boldsymbol{p}_h}{\delta t}(\boldsymbol{x},t) &= \sum_{i=1}^{N_V} \frac{\partial\boldsymbol{x}^i}{\partial t}(t)\varphi_h^i(\tilde{\boldsymbol{p}}_h^{-1}(\boldsymbol{x},t)), \end{aligned} \tag{41}$$

that is, they are time parametrized finite dimensional vectors in V_h and Y_h identified by the coefficients $\{\phi\}'$ and by the control points $\{\boldsymbol{x}\}'$, where the $'$ denotes derivation in time.

We can reconstruct the full discrete gradient $\boldsymbol{\nabla}\phi_h$ on $\Gamma_h(t)$ using the discrete version of the surface gradient $\boldsymbol{\nabla}_s$ and the normal gradient ϕ_{nh}:

$$\begin{aligned} \boldsymbol{\nabla}_s\phi_h(\boldsymbol{x},t) &:= \sum_{i=1}^{N_V} \phi^i(t)\boldsymbol{\nabla}_s\varphi_h^i(\tilde{\boldsymbol{p}}_h^{-1}(\boldsymbol{x},t)) \qquad \text{on } \Gamma_h(t) \\ \boldsymbol{\nabla}\phi_h(\boldsymbol{x},t) &= \boldsymbol{\nabla}_s\phi_h(\boldsymbol{x},t) + \phi_{nh}(\boldsymbol{x},t)\boldsymbol{n} \qquad \text{on } \Gamma_h(t). \end{aligned} \tag{42}$$

In general, the gradients defined in Equation (42) are not necessarily continuous across the edges of the elements K which determine the surface discretization $\Gamma_h(t)$, unless all the basis functions of the space V_h are globally of class $\mathcal{C}^1$. While this is certainly a possibility, it is not strictly necessary to solve a discrete version of Problem (33).

3.1. Iso-parametric discretization

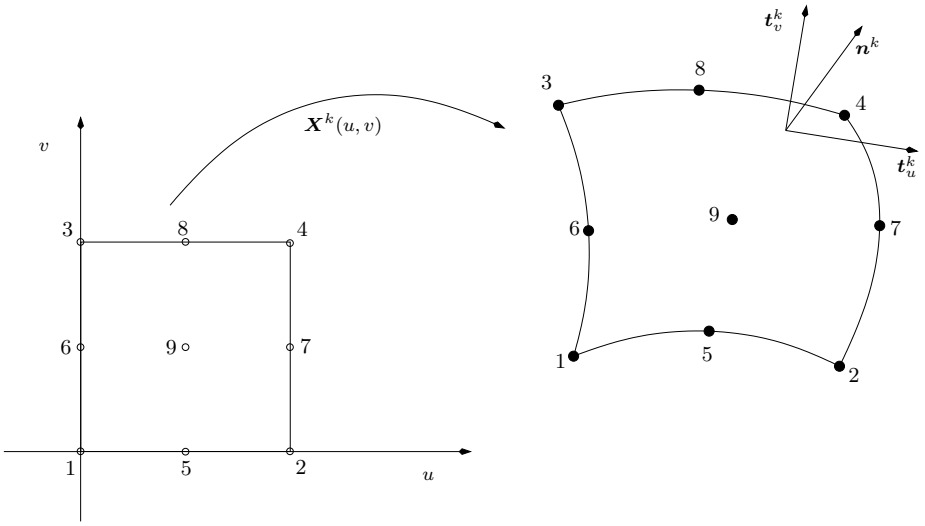

Figure 3: A quadratic panel and the reference element

We approximate the geometry of the domain boundary by means of arbitrary order quadrilateral panels, that is, panels for which the sides and the interior are composed of polynomials and polynomial tensor products respectively.

In particular we define the Lagrangian shape functions $N_l(u,v) \quad l = 1, \ldots, N_L$ on the reference panel (on the left in Fig. 3 we present an example for the quadratic case), which allow us to introduce a local parametrization of the k-th panel as

$$\begin{aligned} \tilde{\boldsymbol{x}}_k(u,v) &:= \sum_{l=1}^{N_L} \tilde{\boldsymbol{x}}^{k_l} N_l(u,v) \qquad\qquad u,v \in [0,1]^2 \\ \boldsymbol{x}_k(u,v,t) &:= \sum_{l=1}^{N_L} \boldsymbol{x}^{k_l}(t) N_l(u,v) \qquad\qquad u,v \in [0,1]^2, \end{aligned} \tag{43}$$

where the weights are the positions of the nodes in the reference domain $\tilde{\Gamma}_h$, or the nodes in the current domain $\Gamma_h(t)$, and k_l is the *local to global* numbering index which identifies the N_L basis functions φ^{k_l} which are different from zero on the k-th panel. The current geometry $\Gamma_h(t)$ is constructed with $\boldsymbol{x}^{k_l}(t)$ instead of $\tilde{\boldsymbol{x}}^{k_l}$, but with the same local parametrization, avoiding the need to explicitly construct the inverse of the map $\tilde{\boldsymbol{p}}(\tilde{\boldsymbol{x}}, t)$, since we rewrite everything in terms of local coordinates on each single panel K.

The global basis functions $\varphi^i(\tilde{\boldsymbol{x}})$ can be identified and evaluated on each panel K via their local parametrization as

$$\varphi_k^i(u,v) := \varphi^i(\tilde{\boldsymbol{x}}_k(u,v)) = \sum_{l=1}^{N_L} \delta_{i\,k_l} N_l(u,v), \qquad \delta_{ij} = \begin{cases} 1 & \text{if } i = j \\ 0 & \text{otherwise.} \end{cases} \tag{44}$$

At this point, a local representation of $\phi(\boldsymbol{x}^k(u,v,t),t)$ and of its normal derivative on the k-th panel are available as

$$\phi_k(u,v,t) = \sum_{l=1}^{N_L} \phi^{k_l}(t) N_l(u,v) \qquad \phi_{nk}(u,v,t) = \sum_{l=1}^{N} {\phi_n}^{k_l}(t) N_l(u,v),$$

where $\phi^{k_l}, {\phi_n}^{k_l}$ $l = 1,\dots,N_L$ are the nodal values of the potential and of its normal derivative in panel k.

There are arguments in favor of selecting a different representation for ϕ_n, based on the consideration that the normals are, in general, not continuous across neighboring panels, but a very reasonable approximation can be obtained, provided that the discontinuities are taken into account where the domain of integration presents sharp features, like corners or edges. In this work, we employ a technique for the treatment of edges and corners developed by Grilli and Svendsen ([13]).

On each point of the panel, it is possible to compute two vectors tangential to $\Gamma_h(t)$ as

$$\boldsymbol{t}_u^k(u,v,t) = \sum_{l=1}^{N_L} \boldsymbol{x}^{k_l}(t) \frac{\partial N_l}{\partial u}(u,v) \qquad \boldsymbol{t}_v^k(u,v,t) = \sum_{l=1}^{N_L} \boldsymbol{x}^{k_l}(t) \frac{\partial N_l}{\partial v}(u,v),$$

from which the external normal unit vector $\boldsymbol{n}$ is obtained as

$$\boldsymbol{n}_{vect}^k(u,v,t) = \boldsymbol{t}_u^k(u,v,t) \times \boldsymbol{t}_v^k(u,v,t), \qquad \boldsymbol{n}^k(u,v,t) = \frac{\boldsymbol{n}_{vect}^k(u,v,t)}{\left|\boldsymbol{n}_{vect}^k(u,v,t)\right|}. \quad (45)$$

The same can be done for vectors tangential and normal to $\tilde{\Gamma}$, by simply replacing $\boldsymbol{x}^{k_l}(t)$ with $\tilde{\boldsymbol{x}}^{k_l}$ in the definitions above. We will denote those vectors with $\tilde{\boldsymbol{t}}_u^k(u,v)$, $\tilde{\boldsymbol{t}}_v^k(u,v)$, $\tilde{\boldsymbol{n}}_{vect}^k(u,v)$ and $\tilde{\boldsymbol{n}}^k(u,v)$, respectively.

Integrals on a panel K (or $\tilde{K}$), can be computed in the reference domain $[0,1]^2$, by observing that $\mathrm{d}\Gamma = J^k(u,v,t)\,\mathrm{d}u\,\mathrm{d}v$, where $J^k(u,v,t) := |\boldsymbol{n}_{vect}^k(u,v,t)|$ (or $\mathrm{d}\tilde{\Gamma} = \tilde{J}^k(u,v)\,\mathrm{d}u\,\mathrm{d}v$, where $\tilde{J}^k(u,v) := |\tilde{\boldsymbol{n}}_{vect}^k(u,v)|$).

Denoting with

$$\begin{aligned}
D_k(u,v,t) &:= \boldsymbol{\nabla}_{uv} \boldsymbol{x}_k(u,v,t) && \in \mathbb{R}^{3\times 2} \\
G_k(u,v,t) &:= D_k(u,v,t)^T D_k(u,v,t) && \in \mathbb{R}^{2\times 2} \\
\tilde{D}_k(u,v) &:= \boldsymbol{\nabla}_{uv} \tilde{\boldsymbol{x}}_k(u,v) && \in \mathbb{R}^{3\times 2} \\
\tilde{G}_k(u,v) &:= \tilde{D}_k(u,v)^T \tilde{D}_k(u,v) && \in \mathbb{R}^{2\times 2},
\end{aligned}$$

where D_k and $\tilde{D}_k$ are the first fundamental forms in the element K and $\tilde{K}$, we can express locally the surface gradient $\boldsymbol{\nabla}_s$ (respectively $\tilde{\boldsymbol{\nabla}}_s$) of the basis functions on K (respectively on $\tilde{K}$) as

$$\begin{aligned}
\boldsymbol{\nabla}_s \varphi^i(\tilde{\boldsymbol{p}}^{-1}(\boldsymbol{x},t)) \mid_{\boldsymbol{x}=\boldsymbol{x}_k(u,v,t)} &= D_k (G_k)^{-1} \nabla_{uv} \varphi_k^i(u,v,t) \\
&=: \boldsymbol{\nabla}_s \varphi_k^i(u,v,t) \\
\tilde{\boldsymbol{\nabla}}_s \varphi^i(\tilde{\boldsymbol{x}}) \mid_{\tilde{\boldsymbol{x}}=\tilde{\boldsymbol{x}}_k(u,v)} &= \tilde{D}_k (G_k)^{-1} \nabla_{uv} \varphi_k^i(u,v) \\
&=: \tilde{\boldsymbol{\nabla}}_s \varphi_k^i(u,v),
\end{aligned} \quad (46)$$

which we will indicate with the same symbol as the spatial surface gradients. The surface gradient of a finite dimensional vector can then be computed by Equation (42).

3.2. Collocation boundary element method

With the iso-parametric representation, the discrete version of the BIE, written for an arbitrary point $\boldsymbol{y}$ on the domain boundary, can be decomposed using the local contributions of the N_L basis functions in each of the M panels of the triangulation:

$$\begin{aligned}\alpha(\boldsymbol{y},t)\phi(\boldsymbol{y},t) = \\ -\sum_{k=1}^{M}\sum_{i=1}^{N_V}\phi^i(t)\int_{\hat{K}}\frac{\partial G}{\partial n}(\boldsymbol{y}-\boldsymbol{x}^k(u,v,t))\varphi_k^i(u,v)J^k(u,v,t)\,\mathrm{d}u\,\mathrm{d}v \\ +\sum_{k=1}^{M}\sum_{i=1}^{N_V}\left(\frac{\partial\phi}{\partial n}(t)\right)^i\int_{\hat{K}}G(\boldsymbol{y}-\boldsymbol{x}^k(u,v,t))\varphi_k^i(u,v)J^k(u,v,t)\,\mathrm{d}u\,\mathrm{d}v. \quad (47)\end{aligned}$$

The numerical evaluation of the panel integrals appearing in equation (47) needs some special treatment, due to the presence of the singular kernels $G(\boldsymbol{y}-\boldsymbol{x})$ and $\frac{\partial G}{\partial n}(\boldsymbol{y}-\boldsymbol{x})$. Whenever $\boldsymbol{y}$ is not a node of the integration panel, the integral argument is not singular, and standard Gauss quadrature formulas can be used. If $\boldsymbol{y}$ is a node of the integration panel, the integral kernel is singular and special quadrature rules are used, which remove the singularity by performing an additional change of variables (see, for example, [18]). In the framework of collocated BEM, an alternative possibility would have been represented by desingularized methods, in which the fundamental solutions are centered at points that are different from the evaluation points. Typically, this is obtained by centering the Green's functions at points that are slightly outside the domain. Although these methods avoid dealing with singular integrals, they pose problems on establishing a general rule for suitable positioning of the fundamental solutions centers. In the case at hand, the domain presents sharp edges and narrow corners (typically found the bow or stern of a hull) which make the latter task nontrivial.

If we write the boundary integral equation for each support point $\boldsymbol{x}^i$, $i = 1,\ldots,N_V$, we can finally recast the discrete version of the boundary integral equation as

$$[\alpha]\{\phi\} + [N]\{\phi\} = [D]\{\phi_n\} \quad (48)$$

where we have used the following notation

- $\{\phi\}$ and $\{\phi_n\}$ are the vectors containing the potential and its normal derivative node values, respectively;
- $[\alpha]$ is a diagonal matrix composed by the $\alpha(\boldsymbol{x}_i(t))$ coefficients;

- $[D]$ and $[N]$ are the Dirichlet and Neumann matrices respectively whose elements are

$$\begin{aligned} D_{ij} &= \sum_{k=1}^{M} \int_{\hat{K}} G(\boldsymbol{x}_i(t) - \boldsymbol{x}^k(u,v,t)) \varphi_k^j(u,v) J^k(u,v,t) \,\mathrm{d}u \,\mathrm{d}v \\ N_{ij} &= \sum_{k=1}^{M} \int_{\hat{K}} \frac{\partial G}{\partial n}(\boldsymbol{x}_i(t) - \boldsymbol{x}(u,v,t)) \varphi_k^j(u,v) J^k(u,v,t) \,\mathrm{d}u \,\mathrm{d}v. \end{aligned}$$

The evaluation of the nodal values for the solid angle fractions α_i appearing in the BIE equation is obtained considering the solution to Laplace problem (23) when $\phi \equiv 1$ in $\Omega(t)$. In this case, system (48) reads

$$[\alpha]\{1\} + [N]\{1\} = 0,$$

which implies

$$\alpha_i = -\sum_{j=1}^{N} N_{ij} \qquad i = 1, \ldots, N. \tag{49}$$

3.3. SUPG stabilization

For the time evolution of the dynamic and kinematic boundary conditions (33b) and (33c), we need to evaluate the surface gradient of the basis functions that appear in Equation (42).

The gradient of the perturbation potential is not, in general, continuous across the edges of the panels that compose $\Gamma_h(t)$, and therefore it is not possible to write directly an evolution equation for the vertices of the triangulation and for the potential nodal values, since on the location of the nodes the forcing term is not single valued.

It is certainly possible to solve this issue by using smooth finite dimensional spaces, as in [12], but this is not strictly necessary. A possible alternative is to impose the evolutionary boundary conditions via an L^2 projection in the V_h space, i.e., we substitute Equations (33b) and (33c) with

$$\left(\frac{\delta\phi}{\delta t}, \varphi\right)_w = (V_\phi, \varphi)_w \qquad \forall \varphi \in V_h \tag{50a}$$

$$\left(\frac{\delta\eta}{\delta t}, \varphi\right)_w = \left(V_\eta, \varphi\right)_w \qquad \forall \varphi \in V_h, \tag{50b}$$

where

$$\begin{aligned} (a,b)_w &= \int_{\Gamma^w(t)} ab \;\, \mathrm{d}\Gamma \\ (a,b) &= \int_{\Gamma(t)} ab \;\, \mathrm{d}\Gamma. \end{aligned} \tag{51}$$

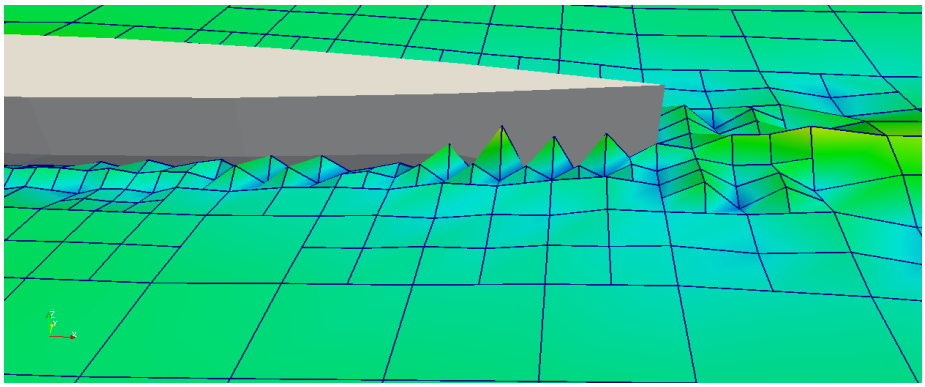

Figure 4: An example of the sawtooth instability developing on the stern of the hull without stabilization.

However, the forcing terms of the evolution equations (34c) and (34d) contain a transport term, respectively $\boldsymbol{\nabla}\eta\cdot(\boldsymbol{w}-\boldsymbol{\nabla}\phi-\boldsymbol{V}_\infty+\boldsymbol{V}_\mathrm{f})$ and $\boldsymbol{\nabla}\phi\cdot(\boldsymbol{w}-\boldsymbol{\nabla}\phi-\boldsymbol{V}_\infty+\boldsymbol{V}_\mathrm{f})$, which becomes dominant whenever $(\boldsymbol{V}_\mathrm{f}-\boldsymbol{V}_\infty)$ is very different from $\boldsymbol{\nabla}\phi$, causing a sawtooth numerical instability which in most cases develops in proximity of the hull stern, with consequent blow up of the simulations (an example of such instability is given in Figure 4).

Once the L^2 projection machinery is in place, as in Eq. (50), a natural and consistent stabilization mechanism that reduces the observed instabilities is the Streamwise Upwind Petrov–Galerkin (SUPG) scheme (see, for example, [15, 24]). In the SUPG framework, the plain L^2 projection in system (50) is replaced by the weighted projection

$$\left(\frac{\delta\phi}{\delta t},\varphi+\boldsymbol{d}\cdot\boldsymbol{\nabla}_s\varphi\right)_w=\left(V_\phi,\varphi+\boldsymbol{d}\cdot\boldsymbol{\nabla}_s\varphi\right)_w\qquad\forall\varphi\in V_h\tag{52a}$$

$$\left(\frac{\delta\eta}{\delta t},\varphi+\boldsymbol{d}\cdot\boldsymbol{\nabla}_s\varphi\right)_w=\left(V_\eta,\varphi+\boldsymbol{d}\cdot\boldsymbol{\nabla}_s\varphi\right)_w\qquad\forall\varphi\in V_h,\tag{52b}$$

where

$$\boldsymbol{d}:=\tau\left(\frac{\boldsymbol{v}-\boldsymbol{w}}{|\boldsymbol{v}-\boldsymbol{w}|}\right),\tag{53}$$

and τ is a positive stabilization parameter which involves a measure of the local length scale (i.e. the "element length") and the local Reynolds and Courant numbers. Element lengths and stabilization parameters were proposed for the SUPG formulation of incompressible and compressible flows in [15], and an in depth study of the stabilization properties for free boundary problems was presented in [24], however, to the best of the authors' knowledge, this is the first time that such stabilization technique is applied directly to a boundary value problem defined on a curved surface.

Expressing everything in terms of the basis functions for finite dimensional space V_h, we get

$$[M][P_{\Gamma^w}]\{\phi\}' = [P_{\Gamma^w}]\{V_\phi\} \tag{54a}$$
$$[M][P_{\Gamma^w}]\{\eta\}' = [P_{\Gamma^w}]\{V_\eta\}, \tag{54b}$$

where

$$\begin{aligned} M^{ij} &:= \big(\varphi^j, \varphi^i + \boldsymbol{d}\cdot\boldsymbol{\nabla}_s\varphi^i\big) \\ &= \sum_{k=1}^{M}\int_{\hat{K}} \varphi_k^j(u,v)\big(\varphi^i(u,v) + \boldsymbol{d}\cdot\boldsymbol{\nabla}_s\varphi^i(u,v)\big)J^k(u,v,t)\,\mathrm{d}u\,\mathrm{d}v \end{aligned} \tag{55a}$$

$$P_A^{ij} := \begin{cases} \delta_{ij} & \text{if } \boldsymbol{x}^i(t) \in A(t) \\ 0 & \text{otherwise} \end{cases} \tag{55b}$$

$$\begin{aligned} V_\phi^i &:= \big(V_\phi, \varphi^i + \boldsymbol{d}\cdot\boldsymbol{\nabla}_s\varphi^i\big) \\ &= \sum_{k=1}^{M}\int_{\hat{K}} V_\phi(u,v)\big(\varphi^i(u,v) + \boldsymbol{d}\cdot\boldsymbol{\nabla}_s\varphi^i(u,v)\big)J^k(u,v,t)\,\mathrm{d}u\,\mathrm{d}v \end{aligned} \tag{55c}$$

$$\begin{aligned} V_\eta^i &:= \big(V_\eta, \varphi^i + \boldsymbol{d}\cdot\boldsymbol{\nabla}_s\varphi^i\big) \\ &= \sum_{k=1}^{M}\int_{\hat{K}} V_\eta(u,v)\big(\varphi^i(u,v) + \boldsymbol{d}\cdot\boldsymbol{\nabla}_s\varphi^i(u,v)\big)J^k(u,v,t)\,\mathrm{d}u\,\mathrm{d}v. \end{aligned} \tag{55d}$$

3.4. Semi-discrete smoothing operator

The semi-discrete version of the smoothing problem (32) can be obtained with a finite element implementation of the scalar Laplace-Beltrami operator, and its application to the different components of $\tilde{\boldsymbol{p}}$.

A weak form of the Laplace-Beltrami operator on $\tilde{\Gamma}$ of a scalar function u in V with Dirichlet boundary conditions u_g on $\tilde{\gamma}$ and forcing term f is given by

$$\begin{aligned} &\left(\tilde{\boldsymbol{\nabla}}_s u, \tilde{\boldsymbol{\nabla}}_s\varphi\right)_{\tilde{\Gamma}} = (f,\varphi)_{\tilde{\Gamma}} && \forall\varphi \in V_0 \\ &u = u_g && \text{on } \tilde{\gamma}, \end{aligned} \tag{56}$$

where we indicate with V_0 the space of functions φ in V such that their trace on $\tilde{\gamma}$ is zero (see, for example, [6] and the references therein for some details on the numerical implementation of the Laplace-Beltrami operator).

The semi-discrete form of Equation (56) can be written as

$$[K]\{u\} = \{F\}, \tag{57}$$

where

$$\begin{aligned} K^{ij} &:= \left(\tilde{\boldsymbol{\nabla}}_s \varphi_h^j, \tilde{\boldsymbol{\nabla}}_s \varphi_h^i\right) \\ &= \sum_{k=1}^{M} \int_{\hat{K}} \tilde{\boldsymbol{\nabla}}_s \varphi_k^j(u,v) \cdot \tilde{\boldsymbol{\nabla}}_s \varphi_k^i(u,v) \tilde{J}_k(u,v)\, \mathrm{d}u\, \mathrm{d}v \\ F^i &:= \left(f, \varphi_h^i\right) \\ &= \sum_{k=1}^{M} \int_{\hat{K}} f_k^j(u,v) \varphi_k^i(u,v) \tilde{J}_k(u,v)\, \mathrm{d}u\, \mathrm{d}v. \end{aligned} \tag{58}$$

The discrete Laplace-Beltrami operator is solved for the auxiliary vector variable $\tilde{\boldsymbol{g}}$, whose finite dimensional representation is given by $\{\boldsymbol{g}\}$, with forcing terms given by the mean curvature along the normal of $\tilde{\Gamma}$.

In this case we write

$$[\boldsymbol{K}]\{\boldsymbol{g}\} = \{\boldsymbol{k}\},$$

where

$$[\boldsymbol{K}] := \begin{bmatrix} [K] & 0 & 0 \\ 0 & [K] & 0 \\ 0 & 0 & [K] \end{bmatrix}$$

$$\{\boldsymbol{k}\} := -2k \begin{Bmatrix} \boldsymbol{n}_x \\ \boldsymbol{n}_y \\ \boldsymbol{n}_z \end{Bmatrix}.$$

and the full semi-discrete version of Problem (33) reads

$$[\alpha]\{\phi\} + [N]\{\phi\} - [D]\{\phi_n\} = 0 \tag{59a}$$
$$[M][P_{\Gamma^w}]\{\phi\}' - [P_{\Gamma^w}]\{V_\phi\} = 0 \tag{59b}$$
$$[M][P_{\Gamma^w}]\{\eta\}' - [P_{\Gamma^w}]\{V_\eta\} = 0 \tag{59c}$$
$$[P_{\Gamma^w}]\{\phi(0)\} - [P_{\Gamma^w}]\{\phi_0\} = 0 \tag{59d}$$
$$[P_{\Gamma^w}]\{\eta(0)\} - [P_{\Gamma^w}]\{\eta_0\} = 0 \tag{59e}$$
$$[I - P_{\Gamma^w}]\{\phi_n\} - [I - P_{\Gamma^w}]\overline{\{\phi_n\}} = 0 \tag{59f}$$
$$[P_\gamma]\{\boldsymbol{g}\}' - [P_\gamma]\{\boldsymbol{w}_g\} = 0 \tag{59g}$$
$$[\boldsymbol{K}]\{\boldsymbol{g}\} - \{\boldsymbol{k}\} = 0 \tag{59h}$$
$$[\mathcal{P}]\{\boldsymbol{g}\} - \{\boldsymbol{x}\} = 0, \tag{59i}$$

where $\mathcal{P}$ is a numerical implementation of the projection operator (34g). On the hull surface, this operator is easily implemented analytically for simple model hulls, such as the Wigley hull. In a more general case, it is desirable to have an implementation of the projection operator that works directly off the CAD files describing the surface.

We implemented both an analytical projection (for the Wigley Hull case) and a CAD based projection, using the OpenCASCADE library [1], although some work is still required to render our full discretization robust with respect to arbitrary hull geometries.

3.5. Time discretization

System (59) can be recast in the following form

$$F(t, y, y') = 0, \tag{60}$$

where we grouped the variables of the system in the vector y:

$$y = \left\{ \begin{array}{c} \{\boldsymbol{x}\} \\ \{\phi\} \\ \{\phi_n\} \end{array} \right\}. \tag{61}$$

Equation (60) represents a system of nonlinear differential algebraic equations (DAE), which we solve using the IDA package of the SUNDIALS Open-Source library [14]. As stated in the package documentation (see p. 374 and 375 in [14]):[2]

> The integration method in IDA is variable-order, variable-coefficient BDF [backward difference formula], in fixed-leading-coefficient form. The method order ranges from 1 to 5, with the BDF of order q given by the multistep formula
>
> $$\sum_{i=0}^{q} \alpha_{n,i} y_{n-i} = h_n \dot{y}_n, \tag{62}$$
>
> where y_n and $\dot{y}_n$ are the computed approximations to $y(t_n)$ and $y'(t_n)$, respectively, and the step size is $h_n = t_n - t_{n-1}$. The coefficients $\alpha_{n,i}$ are uniquely determined by the order q, and the history of the step sizes. The application of the BDF [in Eq. (62)] to the DAE system [in Eq. (60)] results in a nonlinear algebraic system to be solved at each step:
>
> $$R(y_n) \equiv F\left(t_n, y_n, h_n^{-1} \sum_{i=0}^{q} \alpha_{n,i} y_{n-i}\right) = 0. \tag{63}$$
>
> Regardless of the method options, the solution of the nonlinear system [in Eq. (63)] is accomplished with some form of Newton iteration. This leads to a linear system for each Newton correction, of the form
>
> $$J[y_{n,m+1} - y_{n,m}] = -R(y_{n,m}), \tag{64}$$
>
> where $y_{n,m}$ is the mth approximation to y_m. Here J is some approximation to the system Jacobian
>
> $$J = \frac{\partial R}{\partial y} = \frac{\partial F}{\partial y} + \alpha \frac{\partial F}{\partial y'}, \tag{65}$$

[2] We quoted directly from the SUNDIALS documentation. However, we adjusted the notation so as to be consistent with ours and we numbered equations according to their order in this paper.

where $\alpha = \alpha_{n,0}/h_n$. The scalar α changes whenever the step size or method order changes.

In our implementation, we assemble the residual $R(y_{n,m})$ at each Newton correction, and let SUNDIALS compute an approximation of the Jacobian in Eq. (65). The final system is solved using a preconditioned GMRES iterative method (see, e.g., [11]).

Despite the increase in computational cost due the implicit solution scheme, the DAE system approach presents several advantages with respect to explicit resolution techniques. First, it is worth pointing out that among the unknowns in equation (61), the coordinates of all the grid nodes (except for the vertical coordinates of free surface nodes), appear in the DAE system as *algebraic* components, as their evolution is not described by a differential equation, but computed through the smoothing operator. Yet, the time derivative of such coordinates, *i.e.*: the ALE velocity $\boldsymbol{w}$ is readily available through the evaluation of the BDF (62), and can be used in the differential Equations (59b) and (59c) which appear in the DAE system. In particular, at each time step, the convergence of Newton corrections (64) ensures that the vertical velocity of the nodes is the one corresponding to the $\boldsymbol{w}$ velocity originated by the horizontal nodes displacement computed by the smoothing operator. In a similar fashion, the DAE solution algorithm computes the ALE time derivative of the velocity potential at each Newton correction. Such derivative is plugged into Bernoulli's equation (3a) to evaluate the pressure on the whole domain boundary $\Gamma(t)$, without requiring the solution of additional boundary value problems for $\frac{\partial \phi}{\partial t}$. Finally, the resulting pressure field is integrated on the ship wet surface $\Gamma^h(t)$ to obtain the pressure force acting on the ship. As this operation is done at the level of each Newton correction, possible rigid motions of a hull along its six degrees of freedom can be accounted for in a very natural way in the DAE framework, by adding the six differential equations of motion governing the unknown rigid displacements to the DAE system. The latter —strongly coupled— fluid structure interaction model is currently under development and results will be presented in future contributions.

3.6. Adaptive mesh refinement

The main advantages of using a Galerkin formulation for the evolution equation of the free surface, as well as for the computation of the full ALE deformation on the surface $\Gamma(t)$, is two-fold. On one hand, fully unstructured meshes can be used, with an immediate simplification in the mesh generation, and on the other hand, the a posteriori error techniques which are rather popular in the finite element community, can be adopted immediately in this framework, coupled with local refinement strategies, to fully automate the mesh generation and mesh adaptation based on the characteristic of the solution itself, rather than on a-priori heuristic choices.

In this work, we use a modification of the gradient recovery error estimator by Kelly, Gago, Zienkiewicz and Babuska [16, 10], a choice mostly motivated by its simplicity (see [2] for more details on this and other error estimators).

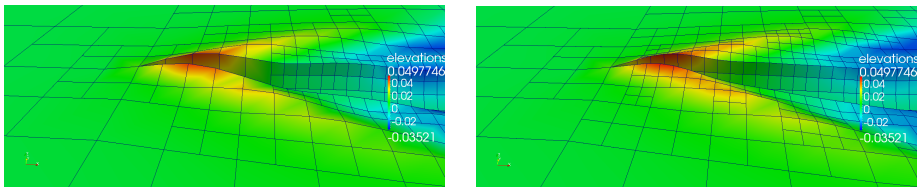

Figure 5: A mesh refinement step.

At fixed intervals in time, the surface gradient of the finite element approximation of ϕ is post-processed to provide a quantitative estimate of where the approximation error may be higher. In particular, for each cell K of our triangulation we compute the quantity

$$\tau_K^2 := \frac{h}{24} \int_{\partial K} \left[\boldsymbol{\nabla}_s \phi \cdot \boldsymbol{n}_{\partial K} \right]^2 \, \mathrm{d}\gamma, \tag{66}$$

where $[\boldsymbol{\nabla}_s \phi \cdot \boldsymbol{n}_{\partial K}]$ denotes the jump of the surface gradient of ϕ across the edges of the triangulation element K. The vector $\boldsymbol{n}_{\partial K}$ is perpendicular to both the cell normal $\boldsymbol{n}$, and to the boundary of the element K, and h is the diamater of the cell itself.

Roughly speaking, τ_K gives an estimate of how well the trial space is approximating the surface gradient of ϕ. The higher these values, the smaller the cells should become. The estimated error per cell τ_K is ordered, and a fixed fraction of the cells with the highest and lowest error τ_K are flagged for refinement and coarsening. The computational grid is then refined, ensuring that any two neighboring cells differ for at most one refinement level.

Standard interpolation is used to transfer all finite dimensional solutions from one grid to another, and a geometrically consistent mesh modification algorithm is used to collocate the new nodes coordinates as smoothly as possible (see [6] for a detailed explanation of this algorithmic strategy). The resulting computational grid is allowed to have hanging nodes, on which the finite dimensional fields are constrained to be continuous. The degrees of freedom associated with the hanging nodes are eliminated from the final system of equations via a matrix condensation technique.

Most of these algorithmic strategies are based on the ones which were already implemented in the `deal.II` finite element library [3] for trial spaces of finite elements defined in two and three dimensions, and were modified to allow their use on arbitrary surfaces embedded in three dimensions. An example of a refinement step is presented in Figure 5.

After each coarsening and refinement step, the system of differential algebraic equations is restarted with the newly interpolated solution as initial condition. A state diagram for the entire solution process is sketched in Figure 6.

4. Numerical simulations and results

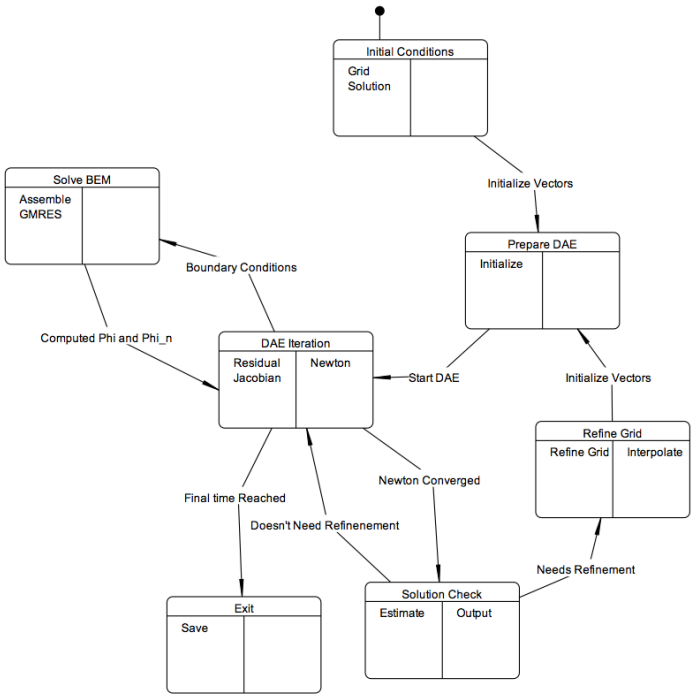

Figure 6: State Diagram

The test case presented in this work is the problem of a Wigley hull advancing in calm water at speed $\boldsymbol{V}_\infty$ parallel to the longitudinal axis, with fixed sinkage and trim. In naval engineering, the Wigley hull is commonly used as a benchmark for the validation of free surface flow simulations. This is mainly due to its simple shape, defined by the equation

$$y(x,z) = \frac{B}{2}\left[1-\left(\frac{2x}{L}\right)^2\right]\left[1-\left(\frac{z}{T}\right)^2\right]. \tag{67}$$

In our simulations the boat length, beam and draft values used are respectively $L = 2.5$ m, $B = 0.25$ m, and $T = 0.15625$ m. A sketch of the resulting hull shape is presented in Fig. 7, which represents a set of vertical sections of the hull.

In the numerical simulation setup, the boat is started at rest, and the its velocity is increased up to the desired speed $\boldsymbol{V}_\infty$ with a linear ramp. The simulation is then carried on until the flow approaches a steady state solution. The presence of the ramp is not needed for the stability and convergence of the solution, which are also obtained imposing an impulsive start of the water past the hull. Still, inducing slower dynamics in the first seconds of the simulations, the linear ramp allows for higher time steps and faster convergence.

To compare the non linear free surface BEM solutions with the experimental

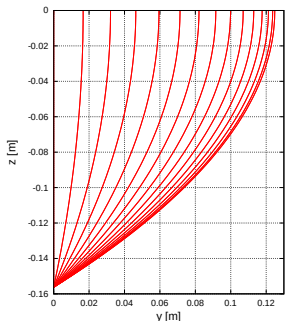

Figure 7: Vertical sections of the Wigley hull used for the simulations, generated by planes normal to the longitudinal axis of the hull.

results presented in [19], we considered six different surge velocities V_∞, corresponding to the Froude numbers reported in Table 1. For each of these Froude numbers, numerical solutions were obtained using a refined and a coarse mesh, in which the adaptive mesh refinement algorithm was tuned in order to maintain the cell dimensions over a given minimum value, and in order to limit the number of degrees of freedom under a maximum value.

V_∞	1.2381 $\frac{m}{s}$	1.3223 $\frac{m}{s}$	1.4312 $\frac{m}{s}$	1.5649 $\frac{m}{s}$	1.7531 $\frac{m}{s}$	2.0205 $\frac{m}{s}$
Fr	0.250	0.267	0.289	0.316	0.354	0.408

Table 1: Wigley hull surge velocities imposed in each numerical simulation, and the corresponding Froude numbers $\mathrm{Fr} = \frac{V_\infty}{\sqrt{gL}}$.

A contour of the wave elevation field for the regime solution obtained at the various Freude numbers is presented in Figures 8, 9 and 10, along with the final mesh. The pictures shows how the adaptive mesh refinement leads to an automatic clustering of mesh cells which captures in very accurate manner the physical characteristics of the wave patterns using a very limited number of degrees of freedom. The final mesh is in fact only composed by roughly 6000 nodes, but it allows for a very good reconstruction of the Kelvin wake, which extends for several wavelengths past the surging hull.

The simulations required 12 hrs (for the coarse meshes) to 48 hrs (for the refined meshes) to reach the steady state solution, on single SMP nodes of the Arctur cluster of the Italian/Slovenian interstate cooperation Exact-Lab/Arctur.

The wave profiles on the surface of the Wigley hull obtained with the present method, are compared with the corresponding experimental results in Fig. 11. In each plot, the abscissae represent the dimensionless coordinate x/L along the boat, while the ordinates are the dimensionless wave elevations $\eta' = \frac{2g\eta}{{V_\infty}^2}$. For all the Froude numbers considered, the method presented seems able to predict qualitatively correct wave profiles. Moreover, the wave elevation in proximity of the bow of the boat is reproduced with very good accuracy in all the test cases considered. On the other hand, in all the numerical curves, we can observe

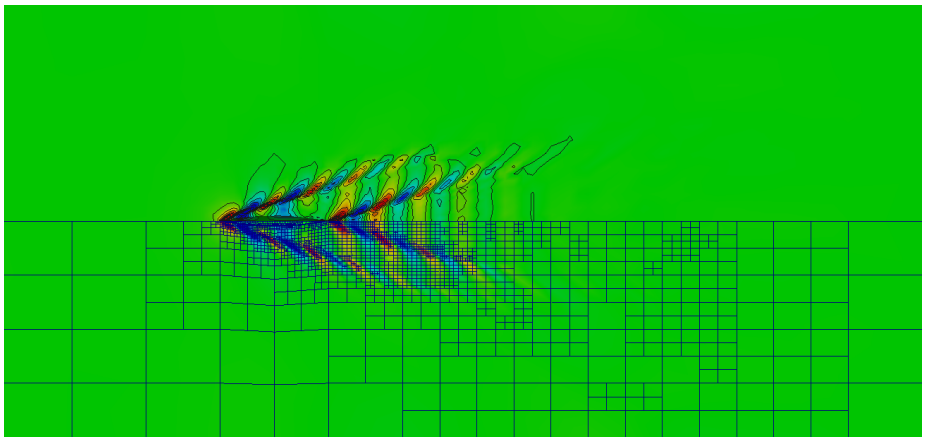

(a) Fr = 0.250

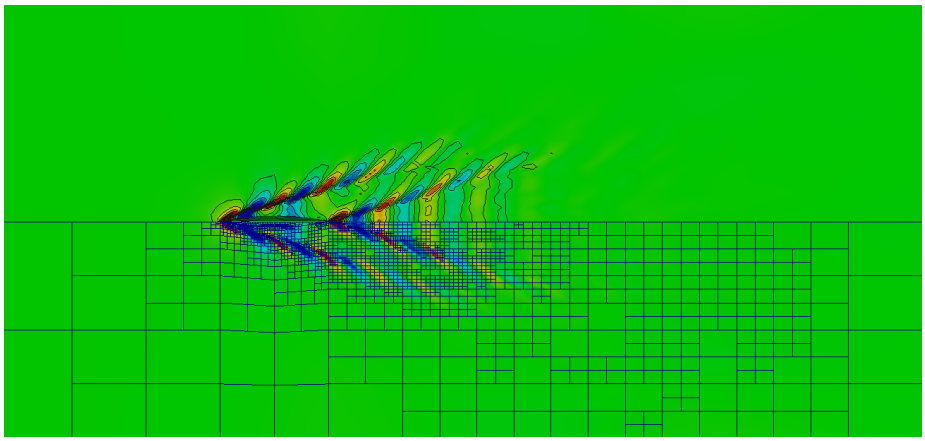

(b) Fr = 0.267

Figure 8: Mesh refinements and contours (I).

a small spatial oscillation superimposed to the main wave profile. The wave length of such oscillation seems proportional to the local mesh cells size, while the amplitude is slightly higher for finer meshes, suggesting that better tuning of the SUPG stabilization parameter may be needed for this kind of boundary value problems.

5. Conclusions

An accurate and efficient boundary element method for the simulation of unsteady and fully nonlinear potential waves past surging ships was developed, implemented and tested. Compared to existing algorithms, the method presents

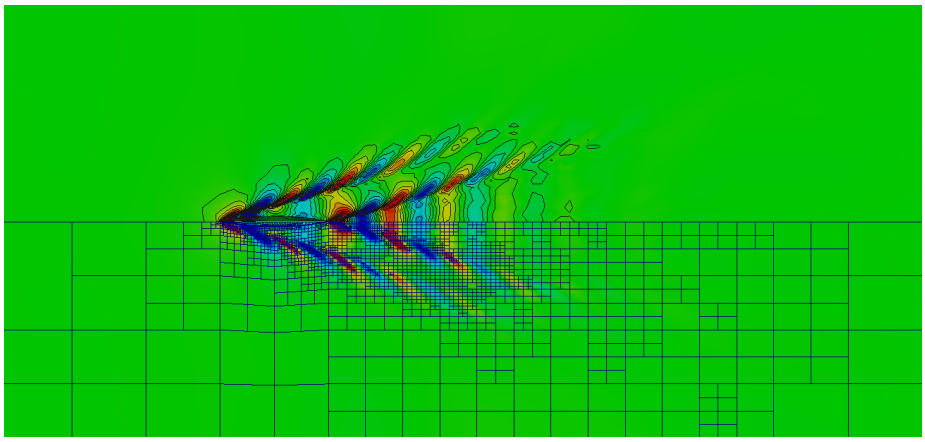

(a) Fr = 0.289

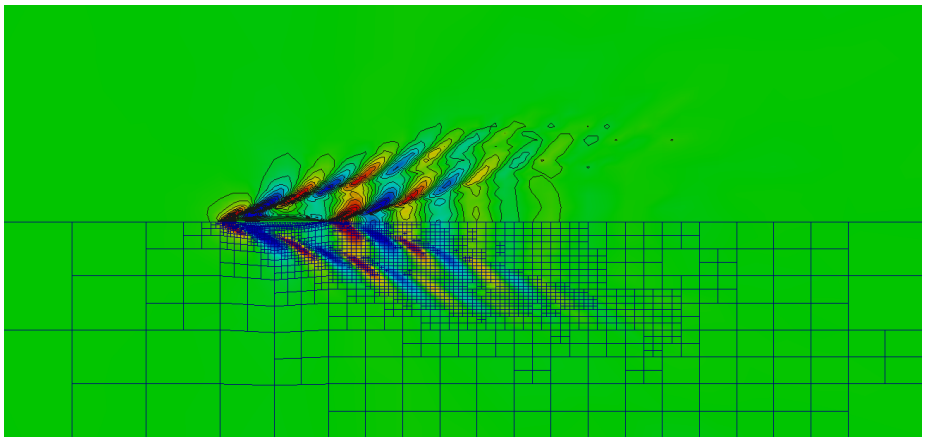

(b) Fr = 0.316

Figure 9: Mesh refinements and contours (II).

several innovative aspects which try to address some of the most CPU intensive aspects of this kind of computations.

The most innovative idea behind the proposed method is the fact that the equations are studied on a fixed reference domain, which is deformed through an arbitrary Lagrangian Eulerian map that keeps track of the physical shape of the water domain around the ship. Some aspects of this approach resemble the semi-Lagrangian formulation of the potential wave equations, but here they are takled using powerful differential geometry tools, combined with finite element techniques for arbitrary surfaces.

This reformulation in terms of a fixed reference domain presents severe stability issues in presence of a forward ship motion, or in presence of an incident stream velocity. Stabilization is achieved via a weighted SUPG projection, which

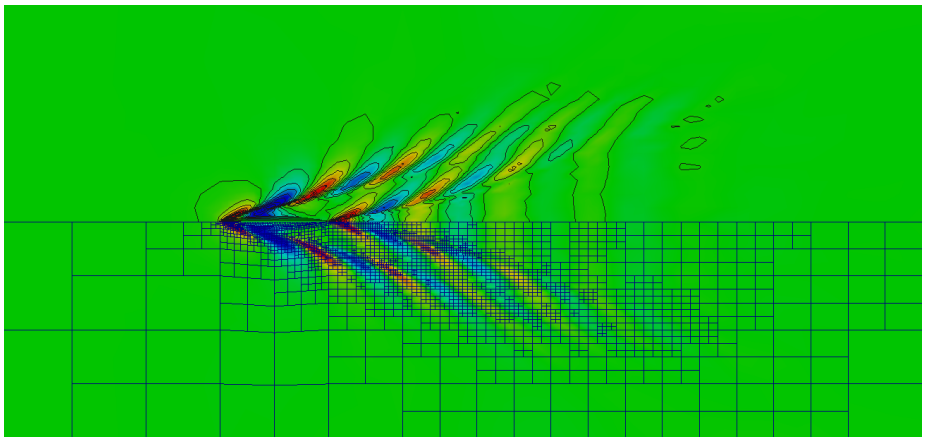

(a) Fr = 0.354

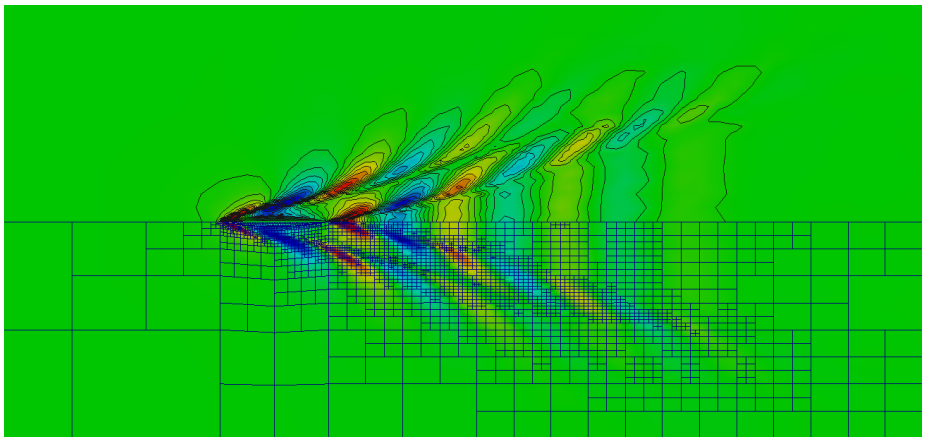

(b) Fr = 0.408

Figure 10: Mesh refinements and contours (III).

allows the use of fully unstructured meshes, and guarantees an accurate reconstruction of the velocity fields on the mesh nodes, also when low order finite dimensional spaces are used for the numerical discretization.

To the best of the authors' knowledge, such formulation has never been successfully used in ship hydrodynamic problems in presence of a non zero stream velocity, due to the free surface instabilities.

With respect to existing methods, the combination of the semi-Lagrangian approach with the SUPG stabilization eliminates the need for periodic remeshing of the computational domain, and opens up the possibility to exploit local adaptivity tools, typical of finite element discretizations.

We exploit these ideas by employing simple a posteriori error estimates to adaptively refine the computational mesh, in order to automatically follow the

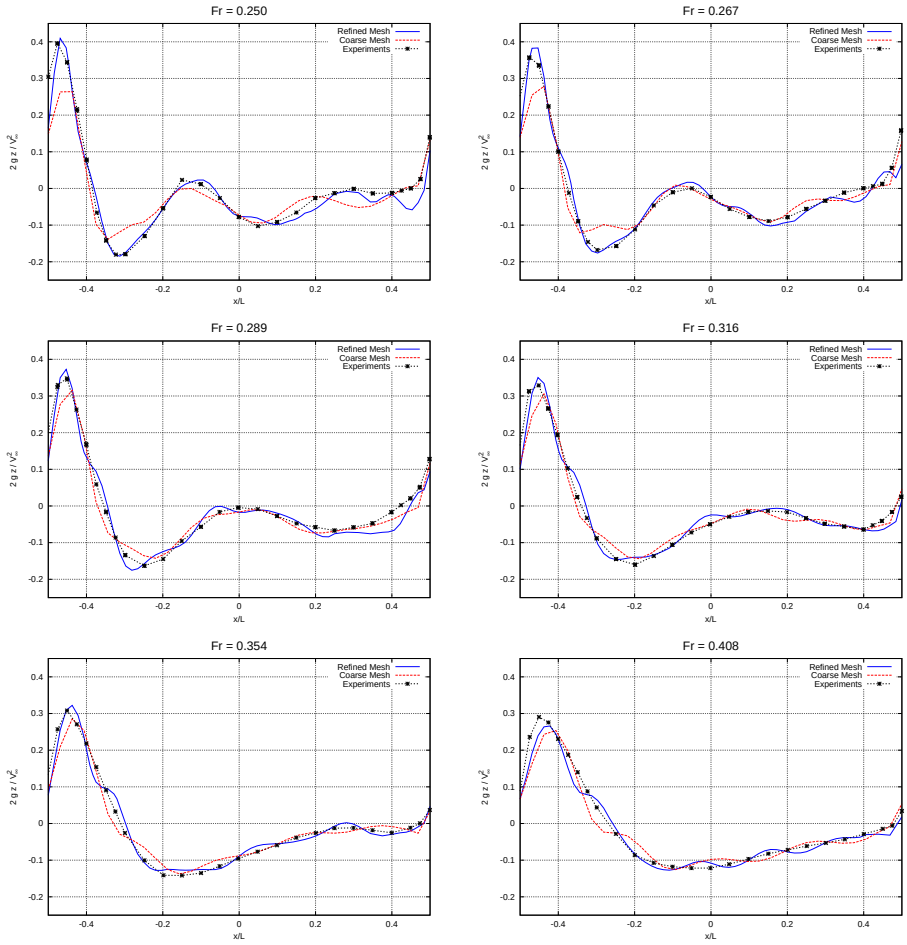

Figure 11: Comparison of predicted water profiles with the University of Tokyo experimental results (- -*- -). Both coarse mesh (– –) and refined mesh results (—) are shown in the plots.

characteristics of the computed solution. Accurate results are obtained even when using a very limited number of degrees of freedom.

Implicit BDF methods with variable order and variable step size are also employed, which render the final computational tool very attractive in terms of robustness.

A direct interface with standard CAD file formats is currently under development, and our preliminary results indicate that the final tool could be used to efficiently study the unsteady interaction between arbitrary hull shapes and nonlinear water waves in a robust and automated way.

Acknowledgments

The research leading to these results has received specific funding under the "Young SISSA Scientists' Research Projects" scheme 2011-2012, promoted by the International School for Advanced Studies (SISSA), Trieste, Italy.

This work was performed in the context of the project OpenSHIP, "Simulazioni di fluidodinamica computazionale (CFD) di alta qualita per le previsioni di prestazioni idrodinamiche del sistema carena-elica in ambiente OpenSOURCE", supported by Regione FVG - POR FESR 2007-2013 Obiettivo competitivita regionale e occupazione.

The authors gratefully acknowledge the Italian/Slovenian cross-border cooperation eXact-Lab/Arctur for the processing power that was made available on the Arctur cluster.

References

[1] OpenCASCADE Technology. `http://www.opencaseade.org`.

[2] M. Ainsworth and J.T. Oden. A posteriori error estimation in finite element analysis. *Computer Methods in Applied Mechanics and Engineering*, 142(1-2):1–88, 1997.

[3] W. Bangerth, R. Hartmann, and G. Kanschat. deal.II – a general purpose object oriented finite element library. *ACM Transactions on Mathematical Software*, 33(4):24/1–24/27, 2007.

[4] R. F. Beck. Time-domain computations for floating bodies. *Applied Ocean Research*, 16:267–282, 1994.

[5] R.F. Beck, Y. Cao, and T.H. Lee. Fully nonlinear water wave computations using the desingularized method. In *Proceedings of the 6th International Conference on Numerical Ship Hydrodynamics, University of Iowa*, 1993.

[6] A. Bonito, R. H. Nochetto, and M. S. Pauletti. Geometrically consistent mesh modification. *SIAM Journal on Numerical Analysis*, 48(5):1877–1899, 2010.

[7] Y. Cao, R.F. Beck, and W. Schultz. An absorbing beach for numerical simulations of nonlinear waves in a wave tank. In *Proceedings of the 8th International Workshop on Water Waves and Floating Bodies, St. John's, Newfoundland*, 1993.

[8] M.C. Delfour and J.P. Zolésio. *Shapes and Geometries: Metrics, Analysis, Differential Calculus, and Optimization*, volume 22. Society for Industrial Mathematics, 2010.

[9] L. Formaggia, A. Quarteroni, and A. Veneziani. *Cardiovascular Mathematics: Modeling and simulation of the circulatory system*, volume 1. Springer Verlag, 2009.

[10] D.S.R. Gago, DW Kelly, OC Zienkiewicz, and I. Babuska. A posteriori error analysis and adaptive processes in the finite element method: Part II–Adaptive mesh refinement. *International journal for numerical methods in engineering*, 19(11):1621–1656, 1983.

[11] Gene H. Golub and Charles F. Van Loan. *Matrix computations*. Johns Hopkins Studies in the Mathematical Sciences. Johns Hopkins University Press, Baltimore, MD, third edition, 1996.

[12] S. T. Grilli, P. Guyenne, and F. Dias. A fully non-linear model for three-dimensional overturning waves over an arbitrary bottom. *International Journal for Numerical Methods in Fluids*, 35:829–867, 2001.

[13] S. T. Grilli and I. A. Svendsen. Corner problems and global accuracy in the boundary element solution of nonlinear wave flows. *Engineering Analysis with Boundary Elements*, 7(4):178–195, 1990.

[14] A. C. Hindmarsh, P. N. Brown, K. E. Grant, S. L. Lee, R. Serban, D. E. Shumaker, and C. S. Woodward. Sundials: Suite of nonlinear and differential/algebraic equation solvers. *ACM Transactions on Mathematical Software*, 31(3):363–396, 2005.

[15] T.J.R. Hughes and A. Brooks. A multidimensional upwind scheme with no crosswind diffusion. *Finite element methods for convection dominated flows*, 34:19–35, 1979.

[16] DW Kelly, D.S.R. Gago, OC Zienkiewicz, and I. Babuska. A posteriori error analysis and adaptive processes in the finite element method: Part I–error analysis. *International Journal for Numerical Methods in Engineering*, 19(11):1593–1619, 1983.

[17] M. Kjellberg, G. Contento, and C.E. Janson. A nested domains technique for a fully-nonlinear unsteady three-dimensional boundary element method for free-surface flows with forward speed. In *21st International Offshore and Polar Engineering Conference, ISOPE-2011; Maui, HI; 19 June 2011 through 24 June 2011*, pages 673–679, 2011.

[18] J.C. Lachat and J.O. Watson. Effective numerical treatment of boundary integral equations: a formulation for three-dimensional elastostatics. *International Journal for Numerical Methods in Engineering*, 10(5):991–1005, 1976.

[19] J.H. McCarthy. Collected experimental resistance component and flow data for three surface ship model hulls. Technical Report DTNSRDC-85/011, David W. Taylor Research Center, 1985.

[20] S. Ryu, M. H. Kim, and P. J. Lynett. Fully nonlinear wave-current interactions and kinematics by a bem-based numerical wave tank. *Computational Mechanics*, 32:336–346, 2003.

[21] S. M. Scorpio. *Fully nonlinear ship-wave computations using a multipole accelerated, desingularized method*. PhD thesis, University of Michigan, 1997.

[22] H. G Sung and S. T. Grilli. Bem computations of 3d fully nonlinear free surface flows caused by advancing surface disturbances. *Journal of Offshore and Polar Engineering*, 18:292–301, 2008.

[23] K. Tanizawa. The state of the art on numerical wave tank. In *Proceeding of 4th Osaka Colloquium on Seakeeping Performance of Ships, Osaka*, pages 95–114, 2000.

[24] T.E. Tezduyar. Computation of moving boundaries and interfaces and stabilization parameters. *International Journal for Numerical Methods in Fluids*, 43(5):555–575, 2003.